UCL Université catholique de Louvain

École polytechnique de Louvain (EPL)

epl

Production of nanostructured ECM-like biointerfaces incorporating bioactive hydroxyapatite nanocrystals

Dissertation presented by
Quentin PAPELOER

for obtaining the Master's degree in
Chemical and Materials Engineering
Option : Biomaterials

Supervisors
Sophie DEMOUSTIER, Christine DUPONT
Co-supervisor
Damien LEFÈVRE

Readers
Charles-André FUSTIN, Étienne FERAIN

Academic year 2016-2017

Abstract

Most of the scientists working in the field of tissue regeneration focus their research on creating a scaffold that allows cells to adhere, proliferate and differentiate. One of the most promising methods up to now consists in mimicking the natural environment of cells, namely the extracellular matrix (ECM). In this work, falling into the bone regeneration field, a new method is presented to synthesise a nanostructured biointerface mimicking the ECM of bone. It is composed of nanotubes made of collagen (Col) and hyaluronic acid (HA), two natural components composing the ECM in the human body. Those nanotubes are synthesised by combining the membrane templated and the layer-by-layer (LbL) methods. Intersected nanotubes are obtained by using track-etched polycarbonate (PC) membranes. In a previous study, mechanically stable systems made of such nanotubes were successfully synthesised by D. Lefèvre by the incorporation of SiO_2 particles. In an attempt to increase the biocompatibility of those systems and to keep their mechanical properties, SiO_2 particles were replaced by another ceramic present in the ECM of bone, the hydroxyapatite (HyAp).

The incorporation of commercially available HyAp nanocrystals within intersected (Col/HA) nanotubes system appeared to be unsuccessful. Indeed, HyAp was discovered to aggregate at the pH used for the LbL synthesis of nanotubes making it difficult to incorporate into the system. However, by *in situ* nucleation of HyAp onto the $(Col/SiO_2)(Col/HA)_n$ system, a crust of HyAp was successfully deposited on the system. In this way, the formation of a biointerface made of intersected nanotubes composed of natural components was well achieved. Still, the mechanical properties have to be improved as the intersected nanotubes of the biointerface collapse.

Acknowledgement

First, I would like to thank my promoters, Sophie Demoustier and Christine Dupont for their availability and their precious advice. They guided me through my research while letting me make my own choices.

I particularly thank Damien Lefèvre for all the time he spent helping and advising me about my work. But also for his fast and precise answers to my questions, his availability, his good mood and for all I learned from him.

I would also like to thank Delphine Magnin for her help concerning the SEM, Elio Poggi for the DLS experiments and his explanations about this technique, Jessem Landoulsi and Elodie Colaço for their invitation to the Pierre and Marie Curie University and the precious information about the hydroxyapatite.

I thank all the members of the BSMA group as well for the good working atmosphere, their availability and the disposable equipment.

Finally, I am also grateful to my family that supports and encourages me during the writing of this thesis.

Table of contents

List of abbreviations

Col	Collagen
***d*-Col**	Denatured collagen
EDC	1-Ethyl-3-(3-dimethylaminopropyl)carbodiimide
ECM	Extracellular matrix
HA	Hyaluronic acid
HyAp	Hydroxyapatite
LbL	Layer-by-layer
OCP	Octocalcium phosphate
PAA	Poly(acrylic) acid
PAH	Poly-(allylamine hydrochloride)
PC	Polycarbonate
PEM	Polyelectrolyte multilayer
PET	Poly(ethylene terephthalate)
PEI	Poly(ethyleneimine)
PLA	Poly(lactic acid)
PLL	Poly($_L$-lysine)
PLLA	Poly($_L$-lactide)
PS	Polystyrene
PSS	Poly(styrene sodium sulfonate)
PVBAC	Poly(vinylbenzylammonium chloride)
SBF	Simulated Body Fluid
SEM	Scanning Electron Microscopy
STEM	Scanning Transmission Electron Microscopy
S-NHS	N-Hydroxysulfosuccinimide
TEM	Transmission Electron Microscopy

Chapter 1

Introduction

During the last decades, the field of tissue regeneration attracted more and more interest. Its aim is to assist the body to recreate the damaged or destroyed tissues without having to replace it. This would prevent organ rejection which is the main problem of transplantation. Moreover, this would solve the problem of shortage of organ donors as they would not be needed anymore.

In the particular case of bone regeneration, within which this thesis falls, one strategy could consist in creating a biointerface on which cells would grow to produce new tissues. By using stem cells collected from the patient, the problem of rejection can be eliminated. The new tissues can be created *in vitro* or *in vivo* if the biointerface is inserted into the body of the patient. One way to allow the interfaces to promote adhesion, proliferation and differentiation of cells is to mimic the extracellular matrix (ECM).

The ECM plays different important roles in the creation of new tissues. Its three-dimensional porous structure acts as a scaffold for cells. It facilitates their localization through the body at precise positions. This scaffold also defines the structure of the newly formed tissue and regulates cell differentiation. The ECM is mainly composed of collagen, elastic fibers, glycosoaminoglycans and proteoglycans as well as adhesive glycoproteins [1]. However, this composition can vary from on tissue to another giving to the ECM different chemical and mechanical properties. The ECM of bone which is especially highly mineralized, is composed of an organic part, giving the elastic properties and an inorganic part, giving the rigidity. The organic part is mainly composed of collagen fibers while the inorganic part is mostly composed of hydroxyapatite.

To mimic the ECM, the electrospinning method was widely used to produce polymer fibers. This technique is fast and easy to set up. However, the polymer choice is limited and natural polymers are difficult to electrospin. Collagen fibers were successfully synthesized by this technique but several modifications of the method had to be done. Moreover, the morphology of the fibers were different depending on the processing conditions [2].

An alternative to this approach could be the templating method combined with the layer-by-layer (LbL) technique. This technique allows to create different types of structure, such as fibers and tubes, made of a wide range of polymers, including natural ones. It consists in creating polyelectrolyte multilayers (PEM) by alternately depositing oppositely charged particles into nanoporous substrates. During the deposition, each polyelectrolyte binds to the other by electrostatic interactions to form a layer, the repetition of these deposition steps leads to multilayers. By carrying out this LbL deposition within the cylindrical nanopores of a template, nanotubes having a similar structure as the ECM nanofibers can be synthesized. Such nanotubes display an internal void space. The great advantage of this hollowness is that nanotubes could be filled using various substances, such as growth factors, which could be released to regulate the behaviour of cells adhered on the biointerfaces.

Those biointerfaces could be used to repair small bone defects due to osteoporosis or unwell repaired fractures. By filling the defects with the biointerface, it would enhance the bone regeneration. They could also be useful when the damages are too wide and that an implant is needed. Indeed, implants are usually metallic which are rather bioinerts. By covering those metallic implants with the biointerface, it would make the implant more biocompatible. Moreover, those biointerfaces would play the role of osteoconductive and osteinductive coatings.

This thesis aims to elaborate a biointerface mimicking the ECM matrix which would regulate the cell behaviour and guide them towards different lineages. Based on the ECM structure, the biointerface is made of intersected nanotubes made of collagen and hyaluronic acid (HA). Those tubes being very soft, the incorporation of a ceramic is needed to improve the mechanical properties of the biointerface and to obtain a mechanically stable system. In a previous work, lead by D. Lefèvre, biointerfaces entirely composed of biopolymers have been produced. However, those had a lack of mechanical stability. Different ways were investigated to enhance the mechanical properties of the interface. It has been decided to incorporate a rigid core to the nanotubes to produce a core-shell structure. One of the strategies investigated was the incorporation of a ceramic, the SiO_2 into the system. It appeared that mechanically stable nanotubes that did not collapse could be obtained. This thesis, that falls into this strategy, aims to replace the SiO_2 by a bioceramic, the hydroxyapatite (HyAp) which composes the major part of natural bones. This bioceramic is known to have good mechanical properties and to exhibit good biocompatibility. It is strong in compression and it promotes cell growth. In this way, the aim to produce a biointerface only made of natural components which would mimic the bone structure would be achieved.

Before exploring the other chapters, all the bibliographic information over the LbL fabrication of nanotubes into nanoporous templates are gathered. The fabrication of collagen and HA multilayers on flat substrates or the fabrication of collagen nanotubes are also described. A deeper description of the three components of the biointerface is also given in this part. Moreover, a special attention is paid to HyAp formation, its interaction with collagen and several of its applications in tissue regeneration.

Next chapter contains all the experimental details to produce and characterize the biointerfaces.

The following part concerns the results and discussion over the fabrication of the biointerfaces. It is composed of two main parts, in the first one, nanocrystals of commercial HyAp were incorporated to the system while in the second one, HyAp was nucleated *in situ*.

In the last section, the main conclusions are summarized and several perspectives to improve or continue this work are proposed.

Chapter 2

State of the Art

This chapter contains bibliographic information related to the production of nanostructured ECM-like biointerfaces incorporating bioactive hydroxyapatite nanocrystals. The first part of this chapter focuses on the methods used to create nanotubes. The template synthesis and the layer-by-layer templating methods are described. Secondly, the growth process of polylectrolyte multilayers is explained. The different characteristics and interactions of collagen and hyaluronic acid are also given to better understand their role in such bioactive systems. Finally, the characteristics of hydroxyapatite and its formation are described to justify its choice as reinforcement and bioactive compound. Several applications containing hydroxyapatite and hydroxyapatite/collagen systems are given to be further compared in Chapter 4 Results and discussion.

2.1 Template synthesis

Introduced by Martin et al. [3] in the 90's, the template synthesis method consists in filling the void space of a porous membrane to elaborate micro- or nano-objects. The pores having a cylindrical shape, fibrils and tubules can be obtained depending on the deposited materials (such as polymers, metals or semiconductors) and the chemistry of the pore wall. Different deposition methods can be used to fill the pores of the membrane like electrochemistry, chemical vapor deposition, sol-gel deposition and LbL adsorption. The material replicates the porosity of the template and can be released by dissolving the membrane.

Another type of template synthesis also exists, which is called the capillary micromolding method. Micromolds are used instead of microporous membranes. They are filled with low-viscosity polymers by capillary action. Finally, patterned films are obtained instead of polymer micro or nanostructures [4].

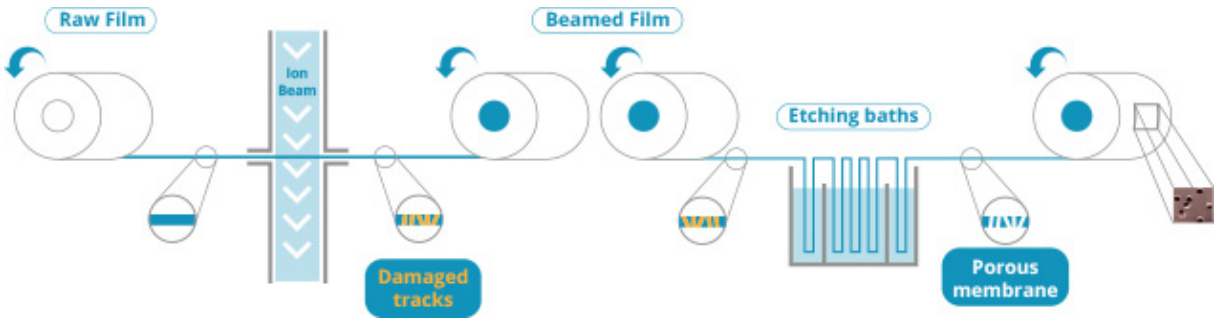

Figure 2.1: Fabrication process of track-etched membranes (taken from `http://www.it4ip.be`).

The versatility of the membrane-templated method offers a large control over the size of the desired structures. Indeed, the outer diameter and the length of the elaborated objects correspond to the pore diameter and the membrane thickness, respectively. It can also be used to functionalize both sides of the nanotubes. The inner side can be functionalized while the nanotubes are still located in the template and the outer side can be functionalized after the tubes are released, when the outer surface is exposed. This allows to obtain a different chemistry inside and outside the tubes.

The choice of the template is an important feature as it mainly defines the structure of the desired nano-objects. It exists two classes, the planar and colloidal templates, both of which can be porous. Planar templates are made of PC or alumina while colloidal templates can be spherical beads of polystyrene (PS) or silica (SiO_2) or nanorods of metals such as nickel, depending on the desired structure. More precise examples of the different templates and some applications are given by Wang et al. [5].

In order to obtain nanotubes or nanorods, two types of planar membranes are mainly used. The first one is a "track-etched" polymer membrane and the second is made of porous alumina. Both are flat surfaces with cylindrical pores. The track-etched method consists in bombarding a polymer membrane with highly energetic ions, which create damaged tracks in the material that can be chemically etched, as depicted on Figure 2.1. At the end, the surface has randomly distributed monodisperse pores. Those membranes can be made of polycarbonate (PC) and poly(ethylene terephtalate) (PET). The pore size can range from 10 nm up to several μm, with a pore density approaching 10^9 pores/cm^2. Figure 2.2 shows a track-etched PC membrane with pore diameter of 1 μm.

Porous alumina membranes are electrochemically prepared from Al metal. The pore density is higher and can reach 10^{11} pores/cm^2 but the range of available pore diameters is more limited [6].

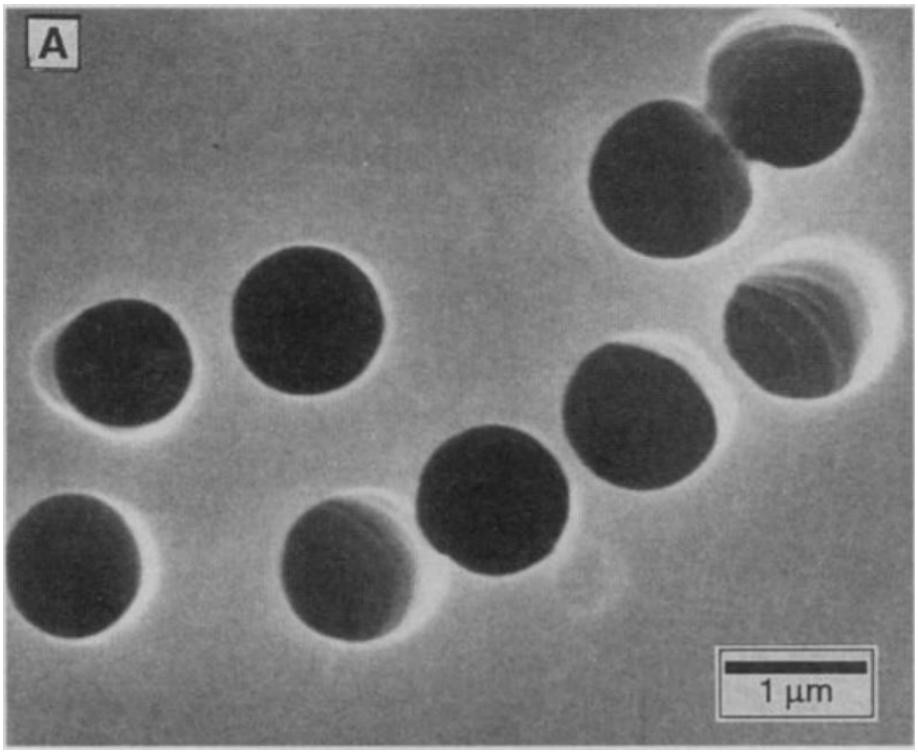

Figure 2.2: SEM image of a surface of a PC membrane with pores 1 μm in diameter (taken from [3]).

2.2 Layer-by-layer templating method

Among the different deposition techniques that can be used to fill nanoporous templates created by the template synthesis, the LbL technique is the simplest and most versatile one. This method consists in alternating two complementary species. A first layer of one species is deposited on the substrate, followed by the deposition of the second one. Due to their complementarity, they form a bilayer on which the first species can deposited again, and so on. By alternating the two species on the substrate, a multilayer is obtained.

The versatility of this technique allows to work with a large choice of compounds and templates. Another advantage of the LbL templating method is that no heavy equipment is required, which makes it a low-cost method.

Nano and micro-objects, created by LbL templating technique, can be composed, among others, of polyelectrolytes, biological macromolecules, dyes, nanoparticles and carbon nanotubes. Different interactions between the compounds can be exploited to create successive layers such as H-bonds, hydrophobic interactions, covalent bonding, complementary base pairing and finally electrostatic interactions which are the most commonly used.

Figure 2.3 shows the different steps of the LbL templating method for polyelectrolytes deposition. First the template is immersed into the polycation solution. During the immersion, the polycation diffuses through the pores and adsorbs on the negatively charged substrate, this correspond to step 1). The adsorption of the polycation changes the electrical charge of the surface which becomes positively charged.

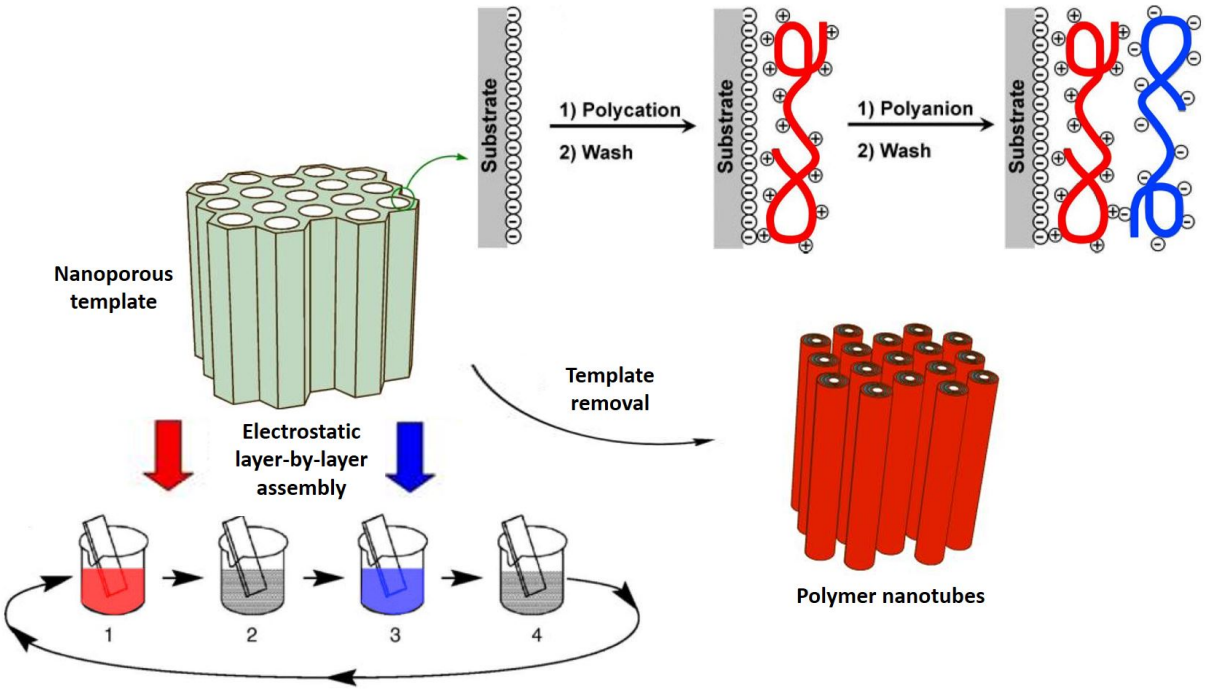

Figure 2.3: Schematic representation of the LbL technique combined with the templating method (adapted from [7] and [6]).

Step 2) consists in rinsing the surface of the membrane to remove unadsorbed materials and to avoid contamination of the other solutions. This can be done by different techniques, simply by washing with pure water or rubbing with sand paper. It is also possible to rinse the inner walls of the pores by filtration of pure water.

During the third step, the membrane is immersed into the polyanion solution. Once the polyanion has diffused through the pores, it adsorbs on the positively charged surface thanks to electrostatic interactions. Owing to an overcompensation of charges, the polarity of the surface changes and a further layer can be added. During the fourth step, similar to the second one, the membrane is rinsed before starting again from step 1).

Those four steps form one bilayer and can be repeated n times to have objects made of n bilayers. Once the desired number of bilayers is reached, the template can be dissolved to release the nano-objects. For example, PC membranes can be dissolved using organic solvents, such as dichloromethane (CH_2Cl_2) [8].

2.3 Growth of polyelectrolyte multilayers

When researchers started their investigations on the growth of polyelectrolyte multilayers (PEM), they first looked into the building of PEM on flat surfaces. With the emergence of the LbL templating method, the study of the growth of PEMs has attracted more and more interest. The different studies showed that the behavior of such PEM is not the same when built up on flat surfaces or into confined systems such as in nanopores. Moreover the differences between the two growth mechanisms are not yet well understood due to the difficulty to characterize the PEM in confined systems.

2.3.1 Growth of PEM on flat substrates

During the deposition of polyelectrolytes on flat substrates, two types of growth mechanisms, i.e. linear and exponential, have been reported. The growth is defined by the increase of the PEM thickness with the number of deposited bilayers. The linear growth involves mainly electrostatic interactions between the polyelectrolytes. Each layer interpenetrates only its direct neighbors, forming a dense film. This growth has been reported for the build-up of poly(styrene sodium sulfate) (PSS) with different polycations such as poly(vinylbenzylammonium chloride) (PVBAC) [8] and poly(allylamine hydrochloride) (PAH) [9]. It has also been reported for systems such as PEI/$(HA/Col)_n$ and is illustrated in Figure (2.4 a) [10].

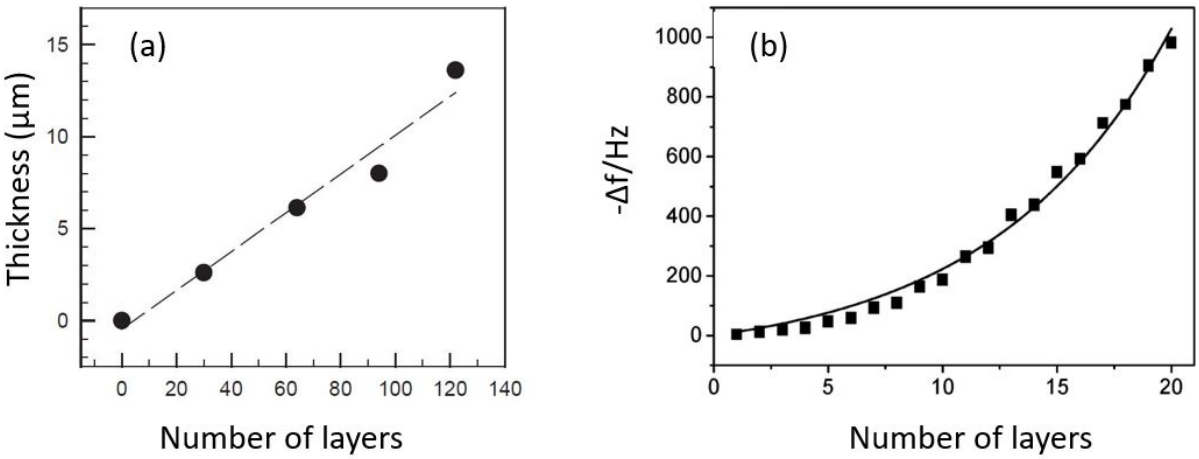

Figure 2.4: Linear growth of PEI/$(HA/Col)_n$ represented by the linear relation between the thickness and the number of bilayers (a) and exponential growth of $(PAH/PSS)_n$ multilayers represented by the exponential relation between the decrease of the frequency shift with the number of bilayers (b) (adapted from [10] and [11], respectively).

In the case of the exponential growth, an "in" and "out" diffusion of some species occurs within the film. It has been demonstrated by Picart [12] that in the case of poly($_L$-lysine) and hyaluronic acid, (PLL/HA) systems, PLL diffuses down to the bottom but also up to the top of the film, whereas HA does not diffuse. In the film, there is a certain proportion of free and bounded PLL chains. When put in contact with the HA solution, the free chains diffuse out of the film to interact with HA. As the chains can come from different lower layers of the film, every new layer increases the number of free PLL chains. More and more PLL diffuses out of the film, leading to an exponential growth. The reasons why HA does not diffuse are not yet well understood but several hypotheses have been made. HA can form a complex network composed of up to 15 chains that interact with each other. HA also has a large persistent length (>10 nm) preventing it from diffusing. This exponential growth has also been reported by Bieker et. al [11] for systems composed of weak polyelectrolytes such as poly(allylamine hydrochloride) (PAH) and polyacrylic acid (PAA). This growth is shown in Figure (2.4 b).

The effect of different parameters on the PEM growth such as the ionic strength, the nature of the substrate and the molar mass have been investigated. For strong electrolytes in low ionic strength solutions, the electrostatic repulsion between the charges of the particles make the chain stiffer, allowing it to adsorb flat on the surface with a minimal amount of loops. On the contrary, when the ionic strength of the solution increases, there is a screening effect which allows the chains to take a random coil conformation. Due to the crumpling of the chains and the presence of loops, the thickness of the adsorbed layer is thicker. A transition from linear to exponential growth can also be induced by an increased amount of salt in the solution. As in the case of strong polyelectrolytes, weak polyelectrolytes form more rigid chains into low ionic strength medium while they are in a random coil conformation in high ionic strength due to the screening of the charges.

However, the behavior of those two kinds of polyelectrolytes with a change in the solution pH is significantly different. While strong polyelectrolytes are fully charged in solution, weak polyelectrolytes are only partially charged and their charge greatly depends on pH. At a pH much above their pKa, anionic polyelectrolytes are almost fully charged while cationic ones have almost no charges on their surface. The opposite is observed for pH much below their pKa. It has been demonstrated by Bieker et al. [11] that the growth of PEM made of weak polyelectrolytes alternates between linear and exponential growth depending on the pH value. This can be explained by the difference of the charge density between the two polyelectrolytes. At low pH (between 3 and 4.5) the poly(allylamine hydrochloride) (PAH), a cationic polyelectrolyte, is almost fully charged while the polyacrylic acid (PAA) has a very small surface charge. PAH forms flat and rigid layer while the PAA forms thicker layer to compensate charges, leading to a linear growth. By increasing the pH between 4.5 and 6, PAH is still almost fully charged but the charge of PAA increases. This leads to a slight charge density mismatch which allows chain diffusion across the layers, leading to an exponential growth. At intermediate pH (between 6 and 8) the two polyelectrolytes have the same charge density and make strong interactions between each other, preventing the diffusion. The growth is again linear. By increasing again the pH from 8 to 10 and then from 10 to 12, the same behavior as described previously happens but the PAA is now almost fully charged and the PAH almost not.

Finally, it appears that the molar mass for both weak and strong polyelectrolytes does not have much influence on the layer thickness. However, in salted solution, the molar mass has a slight effect on the deposited thickness. The nature of the substrate defines whether the surface is positively or negatively charged. Other than that, the substrate nature does not affect the PEM much.

2.3.2 Growth of PEM into nanoporous templates

The growth of PEM into confined systems is known to be different from the one on flat substrates. The deposited layers are thicker in confined system than on flat surfaces, leading to faster pore filling. Moreover, the growth in confined systems depends on the diffusion of the polyelectrolytes into the pores which is not the case for flat substrates. Those systems are also more difficult to characterize as only a few methods can be used to see what happens inside the pores of the membrane.

The fast increase in layer thickness, and thus the fast pore filling, leads to a model where the polymer chains are entangled and form a dense gel. The chains in this gel are in a more concentrated regime where they pile up in the nanopores leading to partial or complete obstruction of the pore. Moreover, this effect may be increased when pressure is applied to the system to force the chains to pass through the pores.

After their investigations on flat substrates, Alem et al. fabricated their (PVBAC/PSS) systems by filtration of the polyelectrolytes through nanopores [8]. A fast increase of the layer thickness has been reported for every tested parameter. The pores were totally filled after only one cycle of deposition. The high local concentration of polyelectrolytes entails the formation of a dense hydrated gel in which the chains are entangled. Because the PEMs swell into aqueous medium, they flatten in the dry state, allowing to obtain nanotubes from fully loaded nanopores in aqueous solution.

Same results were obtained by Roy et al. for their (PAH/PSS) system [13]. Their system was built up by immersion instead of filtration, to avoid the effect of pressure and to better mimic the conditions of the build up on flat substrates. In their work, they evidenced two types of regime. In the first regime, the polymer chains can be represented by hard spheres because their hydrodynamic radius (r_h) is much smaller than the pore diameter. This suggests that the deposition is not limited by the diffusion of the polyelectrolytes in the pores and that the chains adsorb on the pore walls in the same way that they do on flat surfaces. The second regime starts when the pores are almost filled. In this case, the pore diameter becomes close to the r_h and polymer chains cannot be represented by hard spheres anymore. The diffusion of chains through the filled nanopores becomes the growth controlling factor. The chains start to entangle and form the dense gel, also reported by Alem and coworkers [8].

The confined systems are likely to be more sensitive to the nature of the polyelectrolytes and the ionic strength. When a charged particle enters into a nanopore, its charge density can vary from the one in the bulk. This can be due to the higher concentration of polyelectrolyte or to the proximity of the pore walls. Different parameters influencing the growth of PEM such as the ionic strength, the molar mass and the pore diameter have been investigated. Ionic strength increases the layer thickness and can lead to a faster transition to the second regime. Because the system is limited by diffusion, the polyelectrolytes with low molar mass enter the pores more easily and form thicker layers [13]. For the same reason, large pores lead to the formation of thicker layers.

Finally, due to the confinement, there is an intermixing between the layers. Because of the polyelectrolyte proximity, more ion pairing occurs leading to less free charges available for the adsorption of a further layer. After a certain number of bilayers, the charges on the outer surface of the film cannot be overcompensated anymore, preventing the formation of a new layer [6].

2.4 Collagen and hyaluronic acid as natural biopolymers from the ECM

Collagen is the most abundant protein in the human body, it represents approximately 30% of the proteins total mass, 90% of the proteins in the ECM and bones and 50% in the skin. [14]. A typical collagen molecule is a triple helix with a length of 300 nm, a width of 1.5 nm and an approximated molecular mass of 300 kDa. It is composed of three polypeptide chains made of more than 1000 amino acids. Those chains are mainly composed of a repeating unit made of three amino acids, $(\text{Gly-X-Y})_n$, where glycine (Gly) always appears every three amino acid and where the two other ones (X and Y) can vary. Most of the time, X and Y are respectively Proline (Pro) and Hydroxyproline (Hyp), as shown in Figure 2.5 (left). The chains composing the triple helix are bound together by H-bonds which ensures the stability of the molecule.

Up to 28 types of collagen molecules have been found, each of them having the triple helix as building block but showing specific structures and functions. The type I collagen is the most abundant one and will be detailed in this section.[1] The collagen molecules can cross-link with each other to form fibrils with diameters ranging from 10 up to 500 nm, allowing collagen to have complex structures.

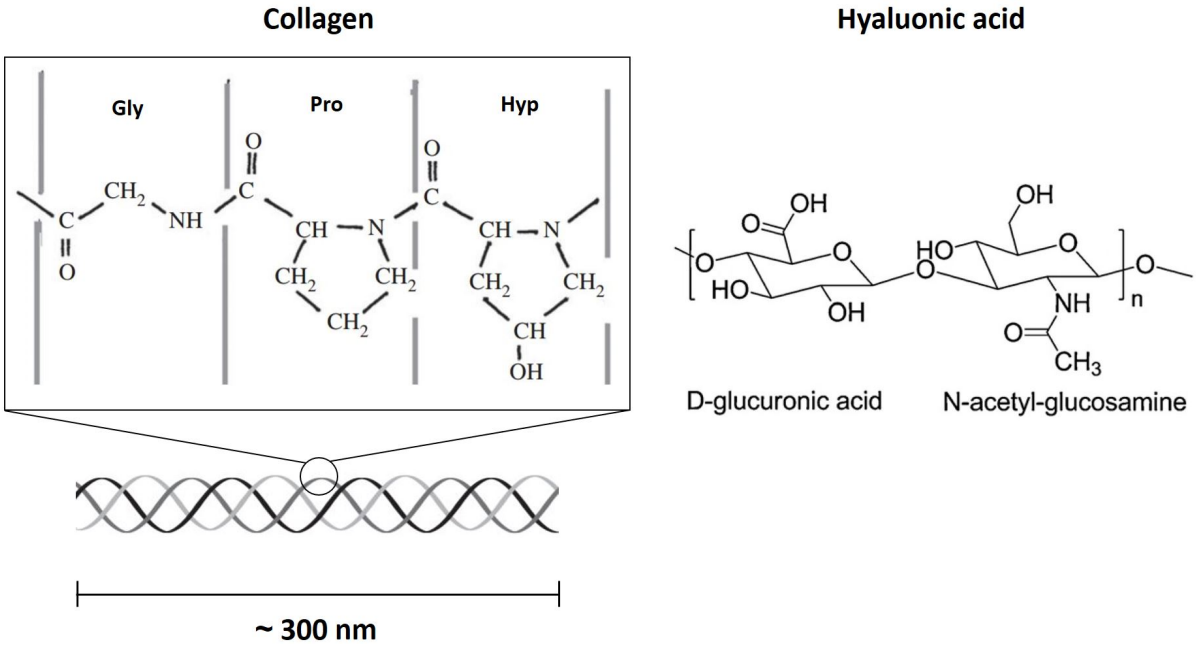

Figure 2.5: Chemical structure of the most abundant repeating unit of collagen (top left, adapted from [15]), collagen triple helix (bottom left, adapted from [16]), and hyaluronic acid (right) [17].

The collagen composition and structure is very similar for all vertebrates. Type I collagen used in research, comes mostly from animal skin and can be isolated by removing the inter-molecular cross-linking using specific enzymes before being purified. Also, collagen has excellent biocompatibility due to its low toxicity and poor immunogenic reaction.

Besides its abundance in the ECM and its different possible structures, collagen is also a good candidate as biomaterial for its numerous interactions with cells and other molecules. Indeed, the collagen structure possesses cells binding domains, it can bind to the α and β subunits of integrins [18]. Scaffolds made of collagen for tissue regeneration (especially for bone tissue engineering) were shown to provide the biological information needed to promote cell adhesion,

[1] Other types of collagen will not be detailed here because they are less interesting regarding the objectives of this thesis.

proliferation and orientation [19]. Moreover, the different carbonyl, hydroxyl and amino groups present in collagen can be functionalized to obtain tailored properties [20].

Yet, collagen also has some drawbacks. As for other natural polymers, it has poor mechanical properties, it is highly hydrophilic and can cause undesired swelling. The purification step may be expensive and there is a potential risk of animal-originated pathogen transmission. However, the advantages explained above overcome those drawbacks in most applications.

Hyaluronic acid is a polysaccharide also abundantly present in the ECM of connective tissues. Half of the HA is located in skin and a quarter in the skeleton, the rest is divided between the muscles and the viscera. It is a glycosaminoglycan composed of a single chain made of disaccharide units composed of D-glucuronic acid and N-acetyl-glucosamine, as shown on Figure 2.5 (right). Hyaluronic acid can be distinguished from other glycosaminosglycans because it does not have nor sulfate nor peptide groups in its primary structure. Besides, its molecular mass is relatively high and can reach more than 8 10^6 Da. Its length offers numerous active sites that can be functionalized to obtain the desired derivatives [17].

H-bonding along the axis of the chain cause a twist in the chain, which imparts stiffness. Thus, the chains take an extended random coil conformation. The twist in the chain also creates hydrophobic sites that allow interactions with other species such as cell membranes or other HA chains, despite the negative charges [21].

Hyaluronic acid also has good viscoelastic properties in the hydrated state. Its elasticity minimizes cell distortion and its viscosity makes it a biological lubricant. Those two phenomena are related to the molar mass and the concentration which needs to be well controlled to obtain the desired properties.

Different applications of HA as a biomaterial, in the field of tissue engineering, cardiac repair, molecule delivery, control of stem cell behavior and others can be found in the review of Burdick et al. [22].

2.5 LbL self-assembly of collagen and hyaluronic acid

2.5.1 (Col/HA)$_n$ system synthesized on flat surface

The build-up of PEM on flat surface using collagen and hyaluronic acid has been reported simultaneously by two research groups. Zhang et al. built Col/HA films on glass slides and quartz wafers, both coated by an anchoring layer made of poly(ethylenimine) (PEI) to form PEI/(Col/HA)$_n$ systems [23]. At the same time, Johansson and coworkers investigated the build-up of Col/HA films on silicon wafer without the help of an anchoring layer [10].

Different conditions have been used to obtain those PEMs. In both cases, the pH was fixed at 4 but the other conditions varied. In the work of Zhang, collagen is diluted into pure water to a final concentration of 0.2 mg/mL while the concentration of HA was 1 mg/mL. Johanson, however, diluted the collagen in an acetate buffer (with the presence of salts) to obtain a concentration of 0.46 mg/mL. The same conditions were used for HA.

As the ionic strength of the medium and the concentration of the polyelectrolytes are known to have a strong impact on their structure, the difference in these parameters can explain the different results obtained. It is also good to note that the substrates were different as well, even if it should not influence the growth mechanism.

The PEI/(Col/HA)$_n$ system was demonstrated to have a linear growth from 0 up to 122 bilayers. Collagen adsorbed on the PEI layer as long and entangled fibers. With further addition of bilayers, the thickness and the length of the fibers increased up to a constant regime.

From their results, Zhang et al. proposed a model in which HA adsorbs on the collagen fibers and overcompensates the charges on the surface. This allows new collagen molecules to adsorb

on the previous layer. It appears that collagen can adsorb along the fibers covered by HA or can deposit itself on the last layer. The first event leads to the increase of the fibers thickness in the lower levels. They increase up to 200 nm after which the collagen cannot diffuse anymore. The second event, however, leads to the formation of a new layer.

The evolution of the ζ potential, which reflects the surface charge of the molecule, with the number of bilayers confirms the electrostatic nature of the interactions occurring between Col and HA. Moreover, the ζ potential oscillates between positive and negative values with a decreasing amplitude up to a constant value [23].

In comparison with what Zhang et al. observed, Johanson and coworkers reported an exponential growth at the beginning of the deposition which tends to be linear for higher number of bilayers. Moreover, HA adsorbs in smaller amount than Col due to its smaller molecular dimensions. Smaller HA molecules adsorb in the form of thin sheets while collagen adsorbs as microfibrils, leading to thicker layers.

The increase in density of the PEM with the addition of Col and its decrease with the addition of HA lead them to a model where the collagen forms a porous layer with a certain thickness in which the HA acts as a mobile species. It creates a complex which makes the structure of the collagen collapse. The superposition of those collapsed films forms the final PEM.

Moreover, the PEM formed with Col and HA are stable at pH 4 but dissolve at physiological pH [10]. At pH 7, collagen approaches its isoelectric point and HA becomes soluble due to the deprotonation of its carboxylic acids. In order to avoid that effect, the PEM is cross-linked with EDC and NHS. After cross-linking, PEM appears to be stable at physiological pH.

2.5.2 Collagen-based nanotubes

The successful build-up of nanotubes made of collagen and hyaluronic acid has not been demonstrated yet. However, Landoulsi et al. [24] created nanotubes based on Col and PSS. PSS is a strong polyanion used to compensate the inhomogeneous charge distribution of collagen ensuring good electrostatic interactions. The nanotubes were fabricated from the LbL templating method. PAH/(PSS/Col)$_6$ nanotubes have been successfully synthesized in a PC membrane with pore diameters of 200 and 500 nm coated by PAH as positively charged anchoring layer. Their external diameter was shown to correspond to the pore diameter and their length corresponds to the PC membrane thickness. The formation of nanotubes depends mainly on the collagen concentration and the diffusion time in the nanopores. Moreover, at least 6 bilayers were needed to obtain mechanically stable nanotubes and the dissolution of the PC membrane by dichloromethane did not alter the nanotubes shape.

In a following study, Landoulsi and coworkers investigated the effect of using native or denatured collagen (d-Col) on their previous system of PAH/(PSS/Col)$_n$ into PC track-etched membrane [25]. The type I collagen molecule is a helix composed of three polypeptide chains stabilized by H-bonds. The denaturation of collagen consists in thermally breaking the H-bonds between the chains. This leads to the formation of simple chains in a random coil conformation, which can easily diffuse through the nanopores of the template.

Formation of PAH/(PSS/d-Col)$_6$ nanotubes was achieved. The outer diameter was observed to correspond to the pore diameter (200 and 500 nm) with a narrow size distribution. The evolution of the thickness increment (Δr) as a function of the number of bilayers measured by gas flow porometry is shown in Figure 2.6.

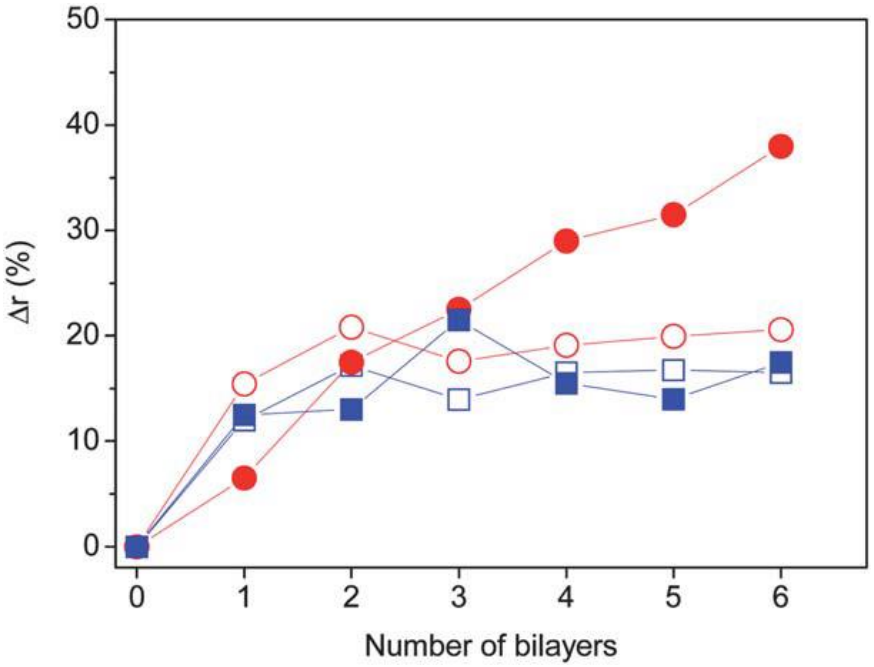

Figure 2.6: Gas flow porometry measurement of PAH/(PSS/Col)$_n$ into PC track-etched membrane: Evolution of the thickness increments (Δr) as a function of the number of bilayer. Pore diameters of 200 nm are represented by circles and pore diameters of 500 nm by squares. Closed and open symbols correspond to *d*-Col and Col respectively (taken from [25]) .

Δr is defined as follows :

$$\Delta r = \frac{d_p(i) - d_p(n)}{d_p(i)} \text{ x } 100$$

where d_p(i) is the initial pore diameter and d_p(n) is the pore diameter measured after the deposition of n bilayers. This parameter allows to compare the growth of the multilayer for small and large pore diameters.

The apparition of a plateau after the deposition of two bilayers indicates that the growth kinetics is slowed down. This suggests that the diffusion of collagen into the nanopores is a limiting factor.

For large pores, the behavior of the *d*-Col is similar to the one of native collagen indicating that a dense structure hindering the diffusion might form. In the case of small pores, the growth of nanotubes composed of denatured collagen is not slowed down and can reach a thickness twice larger than in the other conditions, as it can be seen in Figure 2.6. This phenomenon can be explained by two reasons. First the diffusion of the *d*-Col in the random coil conformation is faster than the one of the filamentous molecules of native collagen. Second, they observed a resolubilization of *d*-Col/PSS on flat surfaces that can still occur in confined systems. Nevertheless, distinguishing the diffusion and the resolubilization effects is not possible with the results obtained above.

The results show the interest of using *d*-Col in small pores when the molecules of native collagen (300 nm) are larger than the pore diameter. However, thermal treatment needed for the preparation of *d*-Col can also alter certain molecular recognition sites, justifying the preference for native collagen.

2.6 Hydroxyapatite as bioactive ceramic

Hydroxyapatite (HyAp) is a ceramic composing the major part of the inorganic component of the bones. It is one of the most stable form of calcium phosphate and it can be found under the form of $Ca_5(PO_4)_3(OH)$ with a Ca/P ratio of 1.67. However, some traces of other components, such as carbonate (CO_3), magnesium (Mg) or sodium (Na) can be found in its chemical structure [26]. HyAp is a brittle ceramic which is strong in compression and weak in tension [27]. Those mechanical properties have been measured on hydroxyapatite monoliths produced in aqueous solution at physiological temperature to obtain the same crystal structure as in bones.

The deposition of HyAp on poly($_{DL}$-lactide) (PDLLA) fibers has been demonstrated to change the mechanical properties of the so formed composite. Cui et al. [20] showed that an increase in HyAp content on PLA fibers increases the tensile strength and the Young's modulus while it decreases the strain at the failure. The stress/strain curves of composites with different HyAp content (HyAp content of d1 < d2 < d3) are represented in Figure 2.7 (taken from [20]). The difference between the d1 and d3 curves shows that the composite mechanical properties change with increasing HyAp content to become stiffer and have less plasticity, which is typical for strong and brittle materials. Hong et al. obtained the same results by incorporation of HyAp into a poly($_L$-lactide) (PLLA) matrix [28].

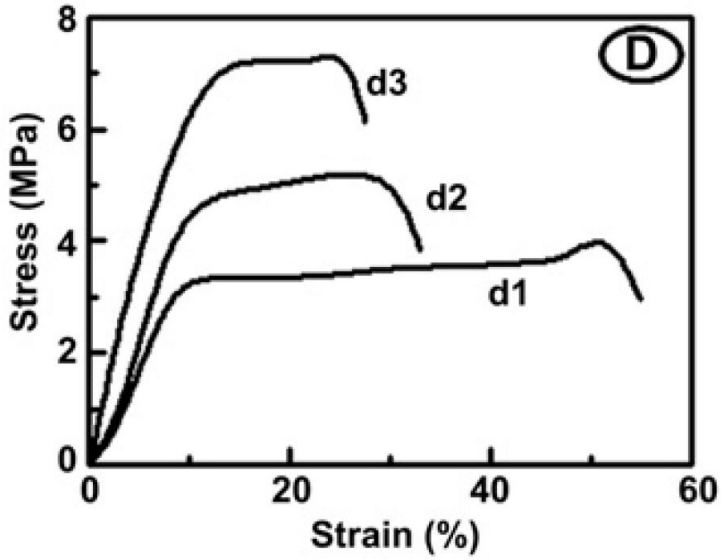

Figure 2.7: Stress/strain curves of PDLLA fibers with a different amount of deposited HyAp (amount of HyAp of d1 < d2 < d3) (taken from [20]).

Moreover, HyAp shows a very good biocompatibility and bioactivity. Meagher et al. [29] proved that HyAp promotes the vascular density, cell density, matrix deposition and mineralization when it is incorporated in a collagen scaffold. They also showed that HyAp promotes the recruitment and the differentiation of endogenous cells to assist the formation of blood vessels and bone in the collagen scaffold. HyAp has been proved to be both an osteoconductive material, as it supports the growth of bone and an osteoinductive material, inducing their formation. The structure of the HyAp has a great influence on those two characteristics. Indeed, it has been proved that the micro (pore diameter smaller than 10 μm) and macro (pore diameter larger than 50 μm) porosity influences the osteoinductivity of HyAp made by calcium phosphate crystals sintering [30].

Due to the importance of the HyAp structure, Sun et al. [31] investigated the influence of the pH on the microstructure of HyAp. They showed that HyAp exhibits nanorods, nanoribbons, needles or spherical shapes with pH varying from 3 up to 11. HyAp is under the form of needles at physiological pH. Those nanoparticles can be used to create composite materials and improve their biocompatibility. Kim et al. [32] developed a new composite made of HyAp nanopowder dispersed into poly(lactic acid) (PLA) and Hong et al. [28] dispersed HyAp particles into PLLA. In both cases, the biocompatibility increased considerably. However, HyAp is rather hydrophilic which induces a low affinity with hydrophobic polymers. In order to obtain a better adhesion between HyAp and the matrix, a surfactant, 12-hydroxysteric acid (HSA), has been used [32] or monomers have been grafted on the HyAp particles [28]. Direct nucleation on a polymer substrate is also an interesting route to avoid adhesion issues between HyAp and its substrate. An alternative method to increase the biocompatibility of a material has been proposed by Elyada et al. [33]. It consists in coating a metallic surface by a PEM to promote the nucleation of calcium phosphate. In this way, the bioactivity of the material is enhanced.

2.7 Hydroxyapatite formation

As briefly mentioned in the previous section, the HyAp can be incorporated into the system by two different ways. On the one hand, HyAp can be crystallized by different methods, then the nanostructured HyAp is incorporated to the system. Its incorporation is done by mixing the HyAp crystals with a polymer matrix to form a composite material [28, 32]. On the other hand, polymer substrates are first created, then HyAp is directly nucleated and grow onto those substrates. The nucleation of HyAp onto polymer fibers [20, 34, 35] or PEMs [33] both have been reported.

2.7.1 Crystallization of nanostructured HyAp

Many different methodologies to synthesize HyAp nanostructures have been proposed. They can be grouped in five types of methods : the dry methods, the wet methods, the high-temperature processes, the synthesis from biogenic sources and combinations of previous methods. However, despite the large panel of available methods, only a few of them are satisfying in terms of economics or performances [36].

The different characteristics of the nanostructures can be tuned by varying the concentration of reagents, the reaction temperature, the aging time and the pH. The shape and the size of the nanocrystals are very sensitive to the temperature and to the concentration of the reagents [26]. The morphology and the nanostructure can be controlled by varying the pH while the crystallinity mostly depends on the aging time and temperature [31]. The different morphologies of HyAp depending on pH are represented in Figure 2.8. Those images have been taken after hydrothermal treatment at 180 °C for 10 h with pH of 3, 5, 7 and 11. At low pH, a flower-like structure of HyAp is obtained. By increasing the pH to a value of 5, the structure becomes a bit more filamentous. HyAp crystals have a needle shape at pH 7, and become more spherical at higher pH.

The natural hydroxyapatite nanocrystals in bones have a needle shape with a width of 15-30 nm and a length of 30-50 nm. Those crystals can be obtained by hydrothermal precipitation of diammonium hydrogen phosphate [$(NH_4)_2HPO_4$] and calcium nitrate tetrahydrate [$Ca(NO_3)_2 \cdot 4H_2O$] at pH 7. The crystals formed by this method are a mixture of HyAp and octocalcium phosphate (OCP). OCP can be removed by increasing the temperature and the pH of the reaction medium [31].

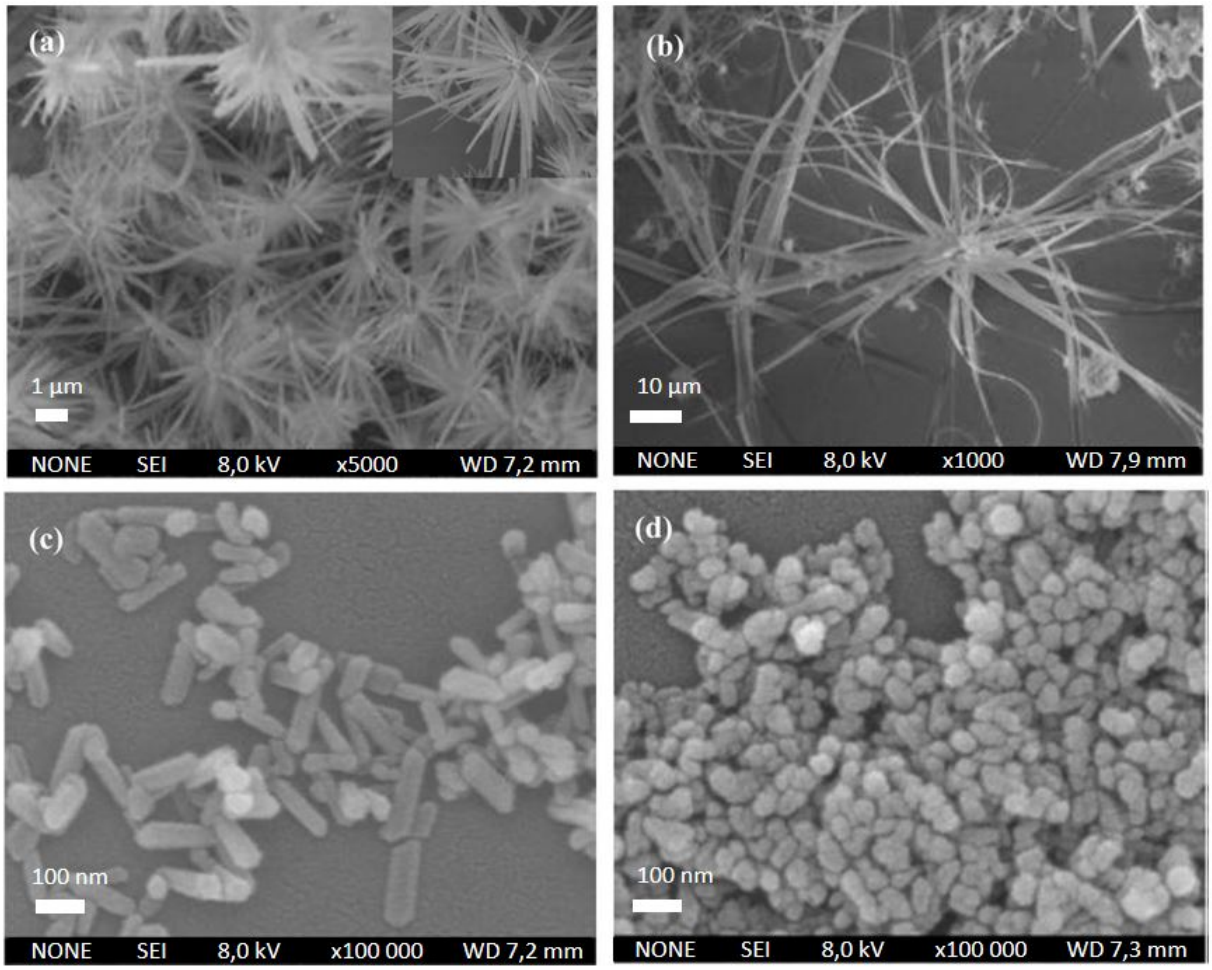

Figure 2.8: FESEM images of HyAp crystals prepared by hydrothermal treatment at 180 °C for 10 h with pH of 3 (a), 5 (b), 7 (c) and 11 (d) (adapted from [31]).

2.7.2 In-situ nucleation of HyAp

Complex structures made of HyAp cannot be directly obtained by the formation of HyAp itself. This is why it is also interesting to nucleate HyAp on a substrate with the desired structure and properties. However, as briefly mentioned previously in the section 2.6, HyAp has a low affinity for most of the polymers. In order to overcome this issue, Tampieri et al. [34] compared the deposition of HyAp nanocrystals and the nucleation of HyAp on collagen fibers. It appears that HyAp deposited itself on collagen fibers by creating randomly dispersed agglomerates without showing any chemical interactions between the two components. On the contrary, the nucleation of HyAp on collagen leads to a homogeneous deposition where the nanocrystals grow parallel to the fiber orientation and show specific chemical interactions with collagen.

The drying method also plays an important role on the final morphology of the final Col/HyAp composite. A 3D network with a very wide pore distribution is obtained by freeze-drying while air-drying method leads to a 2D structure which resembles to the collapsed 3D network.

Finally, it has been demonstrated that Col/HyAp composites created by direct deposition of HyAp nanocrystals are like uncalcified collagen fibers while the nucleation of HyAp on those same fibers gives rise to a system comparable to calcified natural tissues.

The growth mechanism of HyAp nanocrystals on polymer fibers has been investigated by Cui and coworkers [20]. They used PLA fibers that were functionalized by amino, hydroxyl and carboxyl groups. Those three groups have been chosen as they are the most abundant groups

present on the collagen triple helix outer surface. In order to highlight the effect of each group, different densities have been investigated. The adsorption of Ca^{+2} ions on the carboxyl groups is an important feature for the initial step of HyAp formation. Indeed, a large amount of Ca^{+2} around the COO^- attracts the PO_4^- atoms and initiates the nucleation.

The hydroxyl groups have weaker electrostatic interactions with the Ca^{+2} but can still compete for the adsorption. Moreover, the position of this group in the chain can tune the distance between two carboxyl groups. It is thought that when the distance between two carboxyl groups is close to HyAp crystal dimension, the kinetics is accelerated.

The interaction between the amino groups which are positively charged and the carboxyl groups can affect the surface charge. The carboxyl/amino group ratio has then the strongest effect on electrostatic attractions. This can prevent the adsorption of Ca^{+2} on the carboxyl groups and slow the nucleation process.

HyAp nucleation can also be influenced by the surface charge of the substrate. Its nucleation has been successfully achieved on positively and negatively charged surfaces, however, the mechanism is very different [35]. The nucleation on negatively charged surfaces is driven by the adsorption of Ca^{+2} ions from stable solution (meaning that no particle appears in the solution). In the case of positively charged surfaces, the nucleation is only possible in unstable solution where negative particles of calcium phosphate are created. The negative charge is due to the Ca-deficient and phosphate-rich conditions. Those particles adhere on the positively charged surface and start the nucleation.

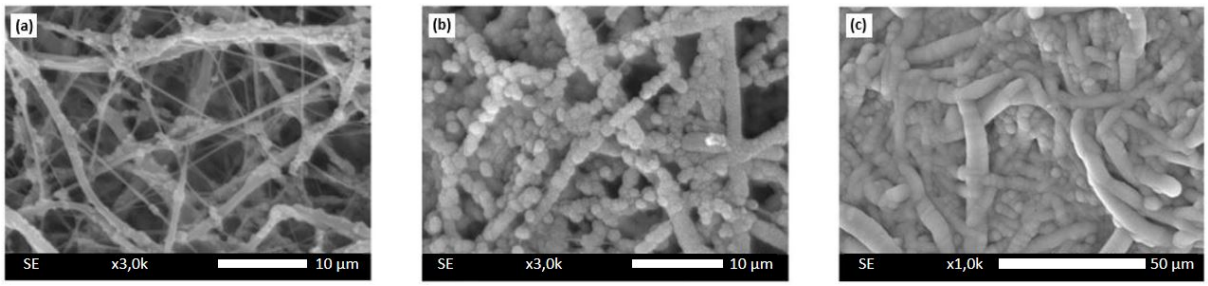

Figure 2.9: SEM images of HyAp nucleated on PCL nanofibers dipped in SBF for 3 (a), 7 (b) and 21 days (c) (adapted from [37]).

The nucleation technique has been used on different substrates. It has been used to cover metal implants [33], polymer nanofibrous webs made of polycaprolactone (PCL) [37] and PLA [20]. The protocol to nucleate HyAp is not always exactly the same but the general features are similar.

Most of the time, the calcium ions come from calcium chloride ($CaCl_2$) and the phosphate comes from disodium hydrogenophosphate (Na_2HPO_4). Yu and coworkers [37] succeeded to nucleate HyAp by a 3-steps method. The first step consists in an activation step, where the PCL web is dipped into an alkaline solution to make the surface negatively charged. The second step is the CaP induction. During this step, the nanofibrous web is dipped successively into $CaCl_2$ and then into Na_2HPO_4 solutions. The last step is the mineralization step where the system is dipped for a couple of days into simulated body fluid (SBF) which contains the same ion concentration as in the human body plasma. In some cases, the induction step is not necessary and the nucleation occurs directly on the negatively charged sites. Figure 2.9 represents SEM images of PCL nanofibers dipped in SBF for 3 (a), 7 (b) and 21 (c) days after the activation and the induction step. The PCL fibers are not fully coated by HyAp after an incubation time of 3 days. On the contrary, after 21 days, HyAp forms a thick coating on the PCL fibers that block the pores. However, after 7 days, the PCL fibers are fully coated and the porous structure is kept.

Based on those results, the optimal incubation time was set to 7 days. The same incubation time was selected in the work of Cui and coworkers [20].

The morphology of the substrate has little effect on the nucleation kinetics. However, in the case of PEMs, the external layer plays an important role as it has to exhibit nucleation sites [33]. The pH plays also an important role as it affects the charge distribution on the surface. In the case of porous membranes, if the change in the surface charge is too large, it can act as an electrostatic barrier and affect the ion diffusion through the pores [38].

2.8 HyAp nanotubes

Nanotubes made of collagen and HyAp have not been reported yet. However, HyAp nanotubes have been created by two different groups of researchers for two different applications. The nanotubes synthesized by Kim and coworkers [39] are shown in Figure 2.10.

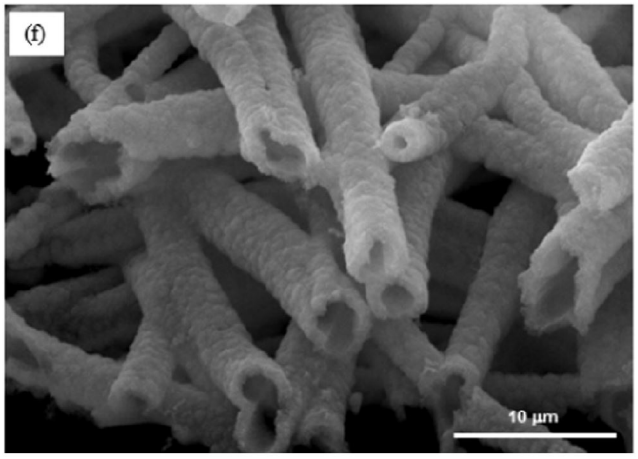

Figure 2.10: SEM images of HyAp nanotubes created by mineralization of PCL electrospun nanofibers and subsequently heat-treated at 800°C (adapted from [39]).

Chandanshive et al. fabricated nanotubes made of a single phase of HyAp in order to mimic the bone structure [40]. To obtain the nanotubes, they used the templating synthesis within an AAO membrane. This porous membrane was dipped into an intermediate Ca-P gel phase, then the system was calcined at 500°C. The release of the tubes was made by dissolution of the AAO membrane. The final nano-objects consisted in hollow tubular structures made of HyAp. Mouse embryonic fibroblast cells were cultured in presence of the HyAp nanotubes to check their biocompatibilty. No change of the cell morphology was observed, suggesting that the tubes are biocompatible.

Contrarily to Chandanshive and coworkers, Kim et al. used HyAp nanotubes for protein delivery [39]. They produced the nanotubes by coating PCL fibers, according to the method of Yu and his group [37] (described in the section 2.7.2). After HyAp deposition, the system was thermally treated at different temperatures. During this step PCL fibers are calcined to obtain hollow structures. Those structures were soaked into a solution containing the proteins. It appears that the amount of adsorbed proteins in the tubes strongly depends on the temperature conditions, lower temperatures showing a higher adsorption. The protein release also depends on the temperature. First, the release is fast and then, the rate slows down until total release. The lower temperatures show a reduced burst at start and the following release is slowed down as well.

2.9 Hydroxyapatite/Collagen systems

In order to better mimic bone structure and function, many researchers focus on Col/HyAp composites. Those materials are promising for bone regeneration as they mimic both inorganic and organic phases of native bone tissue and different applications have already been proposed. However, the exact structure of bone is only roughly mimicked due to the complexity to control all the factors during the formation of the composites.

Two studies investigated the incorporation of HyAp in collagen scaffolds [29, 41]. In both cases, the HyAp/Col composite was shown to exhibit very good biocompatibiliy. The scaffold had the mechanical properties and the structure needed for cell culture. It increased cell proliferation and differentiation compared to scaffolds only composed of collagen. Moreover, it exhibited angiogenesis, remodeling of the scaffold matrix, mineralization and osteogenic gene expression. This makes it a promising candidate for bone regeneration.

Other composites were self-assembled by precipitation of HyAp nanocrystals on fibers [34, 42, 43]. Those composites have a similar nanostructure as bone and a very good biocompatibility has been observed. Moreover, those composites have already been used *in vivo* [43, 44]. It appears that the composite was recognized by the body as an autograft bone and was easily absorbed by the body. Successful clinical trials have been performed [42, 44], making Col/HyAp a very useful and promising material as bone substitute.

More systems containing HyAp and collagen have been produced such as injectable gels [45] and powders for bone substitution and surface coating implant materials [44]. All those different systems and applications show the great interest given to collagen and hydroxyapatite for bone regeneration.

Chapter 3

Experimental section

3.1 Materials

Collagen G type-I (approx. 4 mg/mL) from bovine calf skin was purchased from Merck Millipore. Dried sodium hyaluronate (HA, 151kDa-300kDa) was bought from Lifecore Biomedical. Hydroxyapatite nanoparticles (20-50 nm), 5-10% (w/v) in aqueous colloidal dispersion were purchased from Alfa Aesar. 1-(3-Dimethylaminopropyl)-3-ethylcarbodiimide hydrochloride (EDC), 98+% and calcium chloride ($CaCl_2$), 96% were obtained from Acros Organics. Sodium Chloride (NaCl) ACS reagent $\geq$ 99%, N-Hydroxysulfosuccinimide sodium salt (S-NHS) $\geq$ 98%, sodium phosphate monobasic (NaH_2PO_4) and LUDOX® TM-50 colloidal silica 50 wt. % suspension in H_2O were bought from Sigma-Aldrich.

For the synthesis of individual nanotubes, sheets of track-etched PC membranes were provided by It4ip with pore diameters of 500 nm, a thickness of 21 μm and a pore density of 4 10^7 cm^{-2}. Track-etched PC membranes used to produce systems of intersected nanotubes were provided by It4ip. Two types of membranes have been used, one with pore size of 300 nm with a pore density of 2.8 10^8 cm^{-2} and the second one with pore size of 40 nm and pore density of 1.2 10^{10} cm^{-2}. Both membranes have a thickness of 25 μm and are intersected at an angle of 35-41°.

Hydrophilic PET membranes were also supplied by It4ip, they have a pore diameter of 200 nm with a thickness of 23 μm and a pore density of 5.8 10^8 cm^{-2}.

200 mesh copper holey carbon STEM grids (CF200-Cu) were provided by Electron Microscopy Sciences.

3.2 Solution preparation

All the solutions were freshly prepared before each sample preparation. Only the NaCl solution and the SiO_2 dispersion were reused. The solutions were kept for a maximum of 5 days (approximately the duration of the sample preparation) after what a new one was prepared. All components were diluted into Milli-Q water with 18.2 MΩ·cm resistivity and adjusted at a given pH. The initial pH was adjusted to the desired values with HCl (0.1 M) and NaOH (0.1 M) for collagen and HA solutions and HCl (1 M) for HyAp suspension. The solutions were stirred for 5 to 15 minutes before measuring the pH. Every day, the pH of the solutions was checked and adjusted before use.

Collagen and HA solutions were diluted to obtain a concentration of 1 mg/mL and pH was adjusted to 4 or 5 depending on the experiment. Those pH values have been chosen to be under the isoelectric point of collagen (between 6 and 9.3 [24, 25], it is not well defined due to the complexity of the molecule) and above the pKa of hyaluronic acid (pKa = 2.9 [46]). In this way,

PEM growth is insured because Col is always positively charged while HA is negatively charged. The rinsing solutions were NaCl solutions 150 mM adapted to the same pH as Col and HA solutions during the experiment. The concentration of 150 mM was chosen to be close to the ionic strength of the body fluid. The suspension of SiO_2 1 wt % at pH 4 was already prepared by D. Lefèvre and was reused for all experiments after being stirred for 15 minutes. HyAp was diluted to obtain a dispersion of 0.01%, 0.1% or 1% (v/v) and pH was adjusted to 4 or 5 depending on the experiment. However, HyAp starts to precipitate after a few minutes and needs to be stirred before the filtration.

The solution used to prepare the HyAp *in situ*, was made by mixing $CaCl_2$ with NaH_2PO_4 into Milli-Q water. The final concentrations were $CaCl_2$ 11.4 mM and NaH_2PO_4 6.8 mM to obtain a Ca/P ratio of 1.67.

3.3 Fabrication and release of nanotubes

LbL self-assembly of (Col/HA) multilayers

Nanotubes were synthesized using the templating method combined with the LbL technique. The (Col/HA) multilayers were made by immersion of the PC membrane into the corresponding solutions. The immersion time was 2h for the collagen and 30 minutes for the HA. The longer time for the collagen is due to its structure. The collagen molecules are under the form of cylindrical fibrils, while the HA can take a random coil conformation. HA molecules can be considered to be spherical and can diffuse faster into the pores. Between each new layer, the top and bottom surfaces of the PC membrane were scrubbed in order to remove the polymeric crust and prevent the pore encrusting. The membranes are then rinsed into the salted solutions for 5 minutes to avoid the contamination of the Col and HA solutions. The rinsing of the membranes also allows to desorb molecules that are not well adsorbed into the pores. Indeed, without this step, the unadsorbed molecules could form a soluble complex with the oppositively charged molecules and hinder the adsorption of the next layer. Those steps were similar in the case of intersected systems or simple tubes.

Incorporation of commercial HyAp and strengthening silica nanoparticles within (Col/HA) multilayers

The filtration of both commercial HyAp and SiO_2 dispersion through the PC membrane were performed using the same method. The membrane was placed on a metallic filter[1] attached to the tip of a glass syringe of 1 mL. In total, 5 mL (5x 1 mL) of the dispersions were filtered through the membrane. Before pulling up the piston of the syringe, the filter with the membrane was detached from the tip to avoid a reversal pressure.

When HyAp was deposited by immersion and not filtration, the sample was immersed into pure HyAp for a duration of 24 hours and gently stirred. After the filtration or the immersion step, the membrane was subsequently scrubbed and rinsed for the same reasons explained in the LbL self-assembly of (Col/HA) multilayers.

In situ nucleation of HyAp within (Col/HA) multilayers

The *in situ* nucleation of HyAp was initiated inside simple tubes, inside intersected tubes or on their outer surface. HyAp deposition has been performed by immersion of the system into 10 mL of the solution containing the $CaCl_2$ and the NaH_2PO_4 (named calcifying solution) at different

[1]The filter is only used as a support, its pores are much larger than the one of the PC membrane

stages of the nanotubes formation. When HyAp had to be incorporated into an inner layer of simple tubes or intersected systems, the calcification solution was first adjusted to pH 9 before dipping the PC membrane. On the contrary, when HyAp had to be deposited on the outermost layer of the system, it was first cross-linked and released before being dipped into the calcification solution. The adjustment to pH 9 is performed while the system is already in the solution. After the pH adjustment, the systems were stored for 24 hours in a bath at 37°C in both cases.

Chemical cross-linking of PEMs

The cross-linking was made by mixing 100 mg of EDC and 11 mg of S-NHS into 1 mL of NaCl 150 mM at the same pH used for the other solutions (pH = 4 or 5 depending on the experiments) and then stirred for 5 minutes without heating. The reticulation solution was transfered into a multi-well dish in which the PC membrane was dipped. The dish was wrapped into aluminum film and stored in the fridge for a minimum of two days. After what, the sample was transfered to another well containing NaCl 150 mM at pH 4 or 5 before release.

Release of intersected nanotubes or individual nanotubes from PC membrane

To release the system of intersected nanotubes from the PC membrane, the system was deposited on PET membranes coated by 20 nm of Au or 30 nm of Cr. Then, dichloromethane (CH_2Cl_2) was poured very gently to dissolve the PC without damaging the released system. Finally, the dissolved PC was evacuated by the flow of CH_2Cl_2 while the system stayed on the PET membrane.

When it comes to individual nanotubes, a quarter of the membrane was cut and dipped into 1-2 mL of CH_2Cl_2 to completely dissolve the PC membrane and to release the tubes into the solution. This dispersion is then filtered through PET membranes coated by 20 nm of Au or 30 nm of Cr. In this way, the tubes are deposited on the PET membrane and the dissolved PET is evacuated. During the filtration step, a certain amount of nanotubes are also lost and only a few remain on the surface, allowing a discrete observation of the tubes.

Metalization of the PET membranes

The samples being insulating systems, a conductive layer is needed to prevent the electrons from accumulating at the surface during the SEM observations. The metalization of the PET membranes were done with Cressington Sputter Coater 208HR. The membranes were fixed to a sample holder with double sided tape and then introduced in the sputter coater. Layers of 20 nm of Au or 30 nm of Cr were deposited.

3.4 Characterization of nanotubes

Scanning electron microscopy (SEM), Energy dispersive X-rays (EDX) and Scanning transmission electron microscopy (STEM)

The nanotubes morphology could be determined by SEM. Samples were observed with a JEOL FEG SEM 7600F equipped with an EDX system (Jeol JSM2300 with a resolution < 129eV). The operating conditions were adapted depending on the sample. The majority of them have been observed in SEI mode with an acceleration voltage of 20 kV at a working distance of 6 mm. However, the samples are mainly composed of non-conductive polymers which makes

them difficult to observe with SEM. The accelerating voltage was sometimes changed to 5, 10, 15 or 30 kV depending on the needs.

When EDX analysis was to be done, the acceleration voltage was always the same as for SEM observations but the working distance was set at 8 mm. The acquisition time for chemical spectra varied from 90 to 300 seconds. The analyses of atomic elements were done with the integrated software Analysis Station. For more clarity of the spectrum, the bremsstrahlung was subtracted with the classical "Top Hat Filter" method.

The nanotubes morphology observation by STEM was done in SEM thanks to a STEM detector incorporated in the JEOL 7600F. The instrument was used in TED mode with the same parameters describe above. All STEM images have been taken in bright mode.

Dynamic light scattering (DLS)

The DLS is a non destructive method that uses the light scattering to obtain a size distribution of particles dispersed in a liquid.

A tube containing approximately 1 mL of dispersion is placed at the center of the glass cell containing a liquid with refractive index close to the one of glass. By using this liquid, the temperature of the sample is kept constant. The laser beam, polarized and monochromatic, passes through the system. A part of this laser is scattered by the suspension and is measured by a photodetector placed at an angle θ with the incident beam. In this case, DLS experiments were performed on a Malvern CGS-3 apparatus equipped with a He-Ne laser with a wavelength of 632.8 nm. A schematic illustration is presented in Figure 3.1. The measurements were performed at a 90° angle and each sample was measured at least 3 times in order to check the reproducibility.

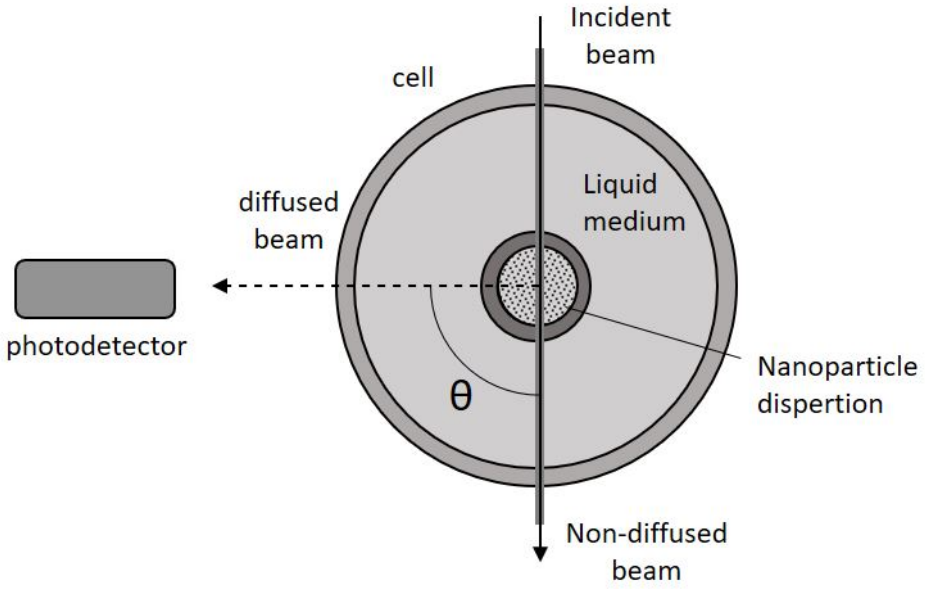

Figure 3.1: Scheme of experimental DLS device viewed from the top.

Particles being in Brownian motion, they move randomly in the solution. When the beam passes through the sample, the signal of the scattered light intensity fluctuates with time and is the results of all the interferences coming from the particles. This signal is analyzed with an auto-correlation function and solved using a Contin algorithm. This method, based on a constraint inverse Laplace transformation of the data, is the most suitable for polydispersed samples.

This gives access to the decay rate (Γ) [s^{-1}] which can be related to the diffusion constant.

$$\Gamma = D \cdot q^2$$

where q is the wave vector [m^{-1}] and D is the diffusion constant [m^2/s].

By using the Stokes–Einstein approximation, the diffusion coefficient can be converted into apparent hydrodynamic radii R_H.

$$R_H = \frac{k_b T}{6\pi\eta D}$$

where k_b is the Boltzmann constant [J/K], T is the temperature [K], and η is the dynamic viscosity of the medium [Pa.s].

It is to note that larger particles diffuse the light more than smaller ones. The signal of large particles is then greater, leading to an "overrepresentation". Because of that issue, the results obtained by DLS cannot be quantitative. Moreover, in the next section, the exact values of the peaks appearing at more than 3000 nm (value chosen arbitrarily, corresponding to 10 times the pore diameter of the PC membranes) are not mentioned. This is because such values show that the system is aggregated and the exact size of the aggregated particles is not relevant in this work.

Chapter 4

Results and discussion

This chapter presents the results and discussion over the different attempts to incorporate HyAp into (Col/HA) systems. The different approaches performed for this purpose correspond to the different sections of this chapter.

The first strategy was to incorporate commercial HyAp nanocrystals into biomimetic system of intersected (Col/HA) nanotubes. In order to do that, different methods were performed. At start, SiO_2 was replaced by HyAp during the nanotubes build-up but HyAp was discovered to aggregate during the nanotube synthesis. Due to this unexpected issue, the influence of the pH on the HyAp aggregation has been studied. The second method investigated to incorporate the HyAp was to adsorb it onto HA instead of collagen. In a final attempt, the HA layers were replaced by a layer of HyAp into collagen nanotubes.

Due to the difficulty to incorporate the commercial HyAp nanocrystals, a second strategy consisting in HyAp incorporation by *in situ* nucleation was also investigated. In a first part, the *in situ* nucleation of HyAp was done inside nanotubes or outside the biomimetic system to see which method was the best. According to the successful results of the incorporation of HyAp outside the intersected system, different methods were investigated to prevent the film from collapsing and obtain a mechanically stable system.

4.1 Incorporation of HyAp nanocrystals into biomimetic systems of intersected (Col/HA) nanotubes

4.1.1 Definition of the controls

In order to compare the results and to define at what point they fit to what is expected, some controls are needed.

In a previous work, D. Lefèvre showed that systems only composed of collagen and hyaluronic acid were not mechanically stable. To rigidify those structures, the strategy was to incorporate silica nanoparticles as rigidifying agent. With this strategy, he successfully produced a mechanically stable $(Col/SiO_2)(Col/HA)_2$ intersected system. To produce it, PC membranes were used with intersected pore of 300 nm in diameter and all solutions were fixed at pH 4.

To emphasize the strengthening effect of silica particles, two controls, a negative and a positive one, were created. The negative control, a $(Col/HA)_8$ system, is only composed of biopolymers. This control would show the lack of mechanical properties related to the biopolymers. The positive control is the same $(Col/SiO_2)(Col/HA)_2$ system than the one produced by D. Lefèvre which would show the gain in stiffness due to the incorporation of silica particles.

This mechanically stable sample is taken as reference (positive control), the objective being to produce samples incorporating HyAp nanocrystals instead of silica nanoparticles while conserving a similar mechanical stability.

Negative control, $(Col/HA)_8$

The production of the negative control lead to the acquisition of a consistent film. Its morphology, observed by SEM is shown in Figure 4.1. The film appears to be flat but can be folded in some places (4.1 a). Some parts of the film have been destroyed and small bundles can be found on the PET substrate (white arrows, 4.1 b). The film is composed of tubular structures (4.1 c) which appears to be compact and aligned. No intersected nanotubes were observed. However, some nanotubes heads are present at the film surface (4.1 d).

The rectangular fragment (4.1 a) and the small white dots (4.1 c) are PC that has not been well dissolved.

The small bundles (4.1 b) due to the partial destruction of the film show that it is not very resistant and that it lacks mechanical properties. Moreover, the dense and rather aligned morphology of the tubular structures is typical for this kind of collapsed system. Indeed, the nanotubes in the system form a mesh and when it collapses, it creates a kind of mat composed of tubes aligned side by side.

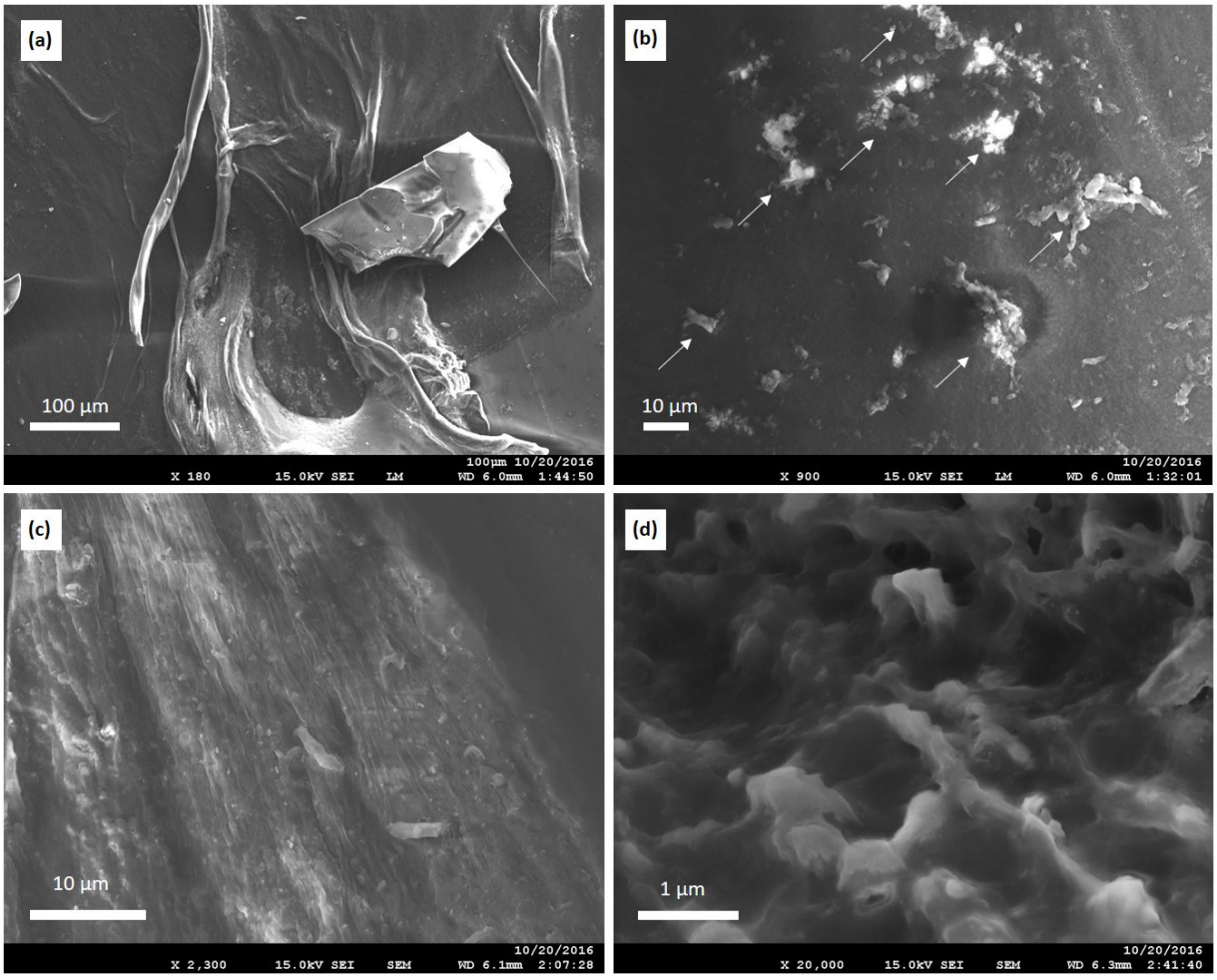

Figure 4.1: SEM images of sample $(Col/HA)_8$ showing the self assembled film (a), part of the destroyed film (white arrows, b), the aligned tubular structures (c) and the nanotubes heads (d).

Positive control, $(Col/SiO_2)(Col/HA)_2$

The morphology of the sample $(Col/SiO_2)(Col/HA)_2$ has been observed by SEM and can be seen in Figure 4.2. The build-up of this system leads to the formation of a film composed of intersected tubular structures with a thickness of several microns. However, some intersected nanotubes can be seen between them (white circle on (4.2 a)). To see them better, a zoom is presented on the picture (4.2 b). Salt crystals with their typical cubic structure can also be seen on those two images. Other particles having a more spherical shape are also present (4.2 c). Those are believed to be PC which has recrystallized after dissolution. Finally, a closer look on the nanotubes shows the presence of the small silica particles (4.2 d) incorporated within the nanotubes.

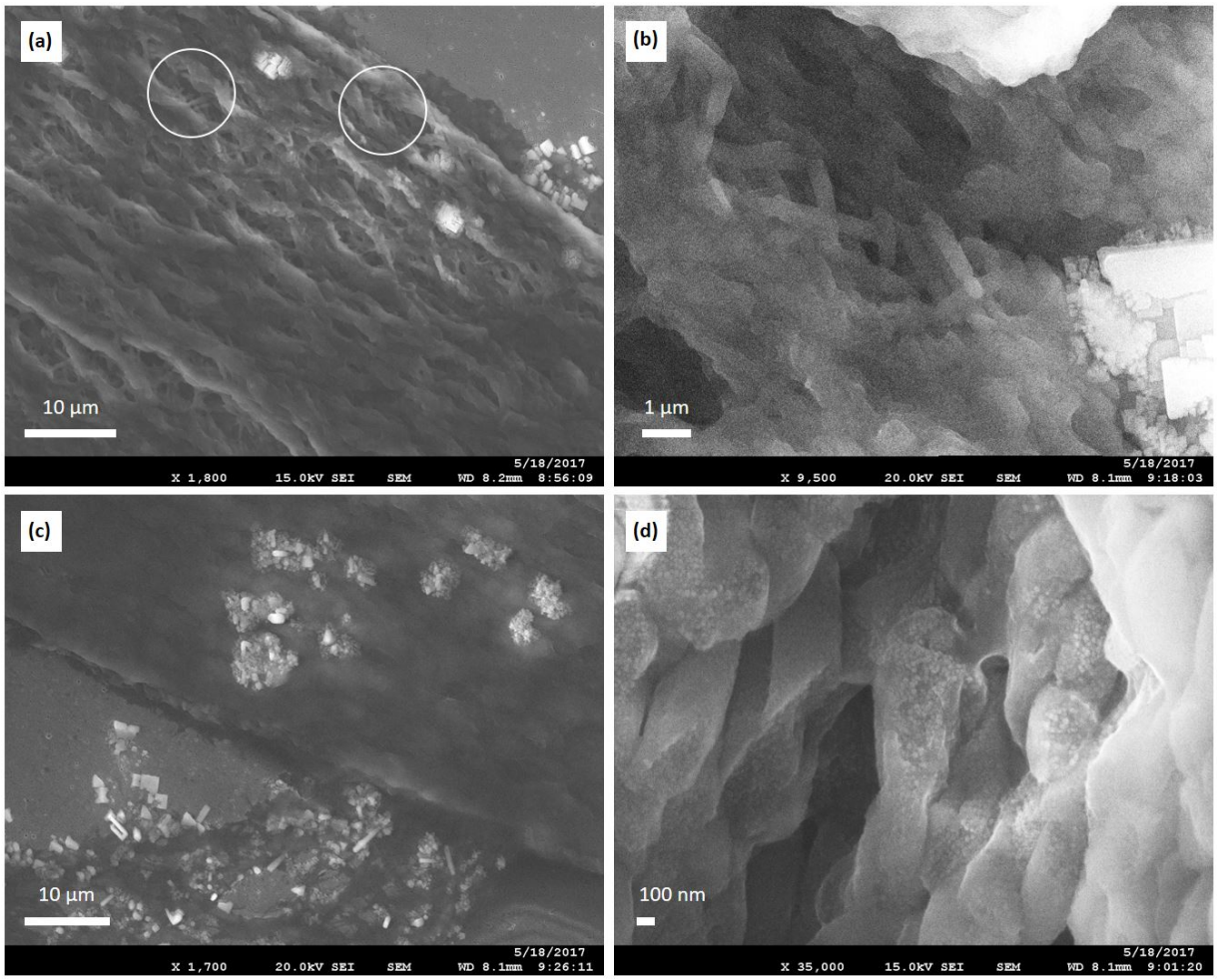

Figure 4.2: SEM images of the reference sample $(Col/SiO_2)/(Col/HA)_2$ showing tubular structures (a), intersected nanotubes (b), remaining PC on the film (c) and SiO_2 particles (d).

The thickness of the sample is only a few microns and not around twenty, as expected from the thickness of the templating PC membrane. This leads to the conclusion that the film is made of collapsed nanotubes and is not mechanically stable. Salt is present in all solutions used for the fabrication of nanotubes. It is not surprising to find it on the sample. Some of the crystals have a larger size than the pore diameter, demonstrating that salt crystallized during the drying step after the releasing step. Besides, despite the fact that the same method was used, the results are different than those obtained by D. Lefèvre, showing the complexity of such fragile systems. The trickiest part of the synthesis protocol is the release process because the tubes are no more supported by the PC membrane. The collapsing of the film may be due to the pressure applied

locally during the drop-by-drop pouring of the CH_2Cl_2. The height and the flow are hard to control as it is done manually. Moreover, due to the complex structure of the system, CH_2Cl_2 has to diffuse through the film to dissolve the membrane. The concentration of CH_2Cl_2 is then not the same everywhere, leading to a heterogeneous dissolution. The presence of the PC remaining on the film is in agreement with this hypothesis.

However, this sample is consistent as control because it still forms a thin porous film made of tubular structures composed of Col and HA. This corresponds to a favorable environment for cells to adhere and proliferate.

By comparing the two controls, the $(Col/HA)_8$ film is more fragile than the $(Col/SiO_2)(Col/HA)_2$ one, even if the number of bilayers was greatly increased. This already shows the great impact of the silica particles on the stiffness of the system. Moreover, the mat composed of aligned tubes that was obtained after the film collapse could explain why both structures are made of tubules that are thicker than the nanotubes. The tubes being composed of 8 bilayers, in the case of $(Col/HA)_8$ their wall thickness [1] is larger than $(Col/SiO_2)(Col/HA)_2$ and create a denser film when it collapses. The denser film may also be due to the incomplete dissolution of the PC membrane which does not release totally the tubes.

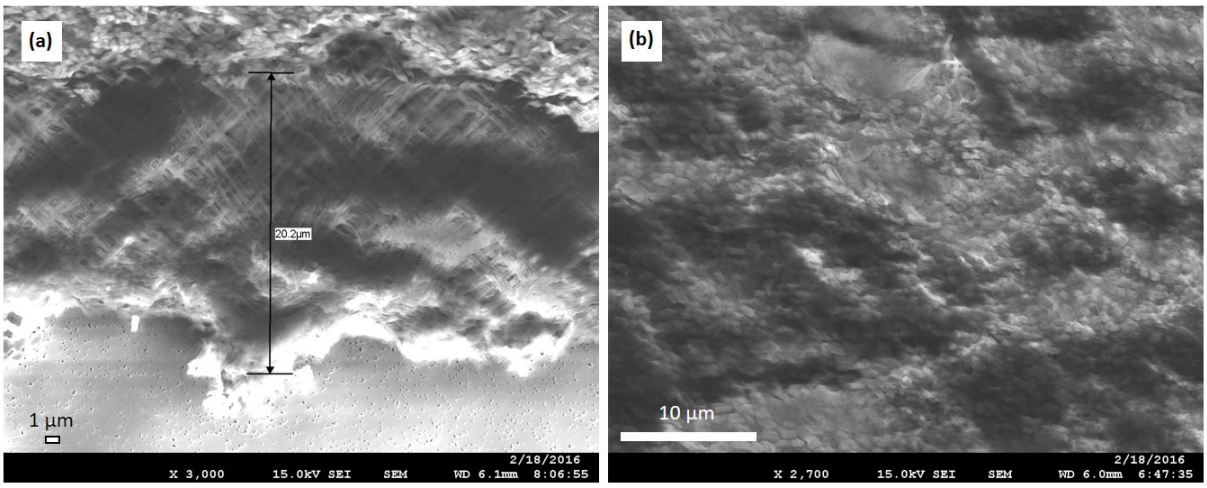

Figure 4.3: SEM image of the $(Col/SiO_2)/(Col/HA)_2$ system synthesized by D. Lefèvre showing one edge of the film composed of intersected nanotubes (a) and its surface composed of nanotube heads (b). Those images were provided by D. Lefèvre.

In any case, the build-up of systems made of collagen and hyaluronic acid creates a film made of tubular structures. In the following sections, the systems will be defined as "successful" when a mat of tubular structures is obtained and when nanotubes can be observed. The production of a mechanically stable system would be a must but due to the complexity to obtain such structure, it is not a necessary condition for the film to be successful. Indeed, by looking at the possible applications for this biointerface, it would be interesting to already study the cell behavior towards those biointerfaces being collapsed or not. Figure 4.3 shows the mechanically stable $(Col/SiO_2)/(Col/HA)_2$ system synthesized by D. Lefèvre. The thickness of the film corresponds to the one of the PC membrane (21 μm) and the intersected nanotubes are clearly seen (4.3 a). On the second image (4.3 b), nanotube heads on the surface of the film can be observed. Those results correspond to what should be obtained when mechanically stable systems are expected.

[1] The diameter of the tubes are the same in both cases because it is defined as the pore diameter of the PC membrane which is equal to 300 nm.

4.1.2 Incorporation of commercially available HyAp nanocrystals into biomimetic (Col/HA) nanotubes

The first idea to incorporate HyAp into the system was to replace the SiO_2. The same conditions as the ones for the control $(Col/SiO_2)(Col/HA)_2$ were used to produce the sample $(Col/HyAp)(Col/HA)_2$. The PC membrane had an average pore diameter of 300 nm and the HyAp concentration was of 1 % (v/v) fixed at pH 4. In the same time, two other samples were made to investigate the impact of the pore diameter and the effect of the HyAp addition. Those two samples were created in the same conditions as explained before except that the PC membrane had a pore diameter of 40 nm, which is smaller than the length of the collagen molecule (300 nm).

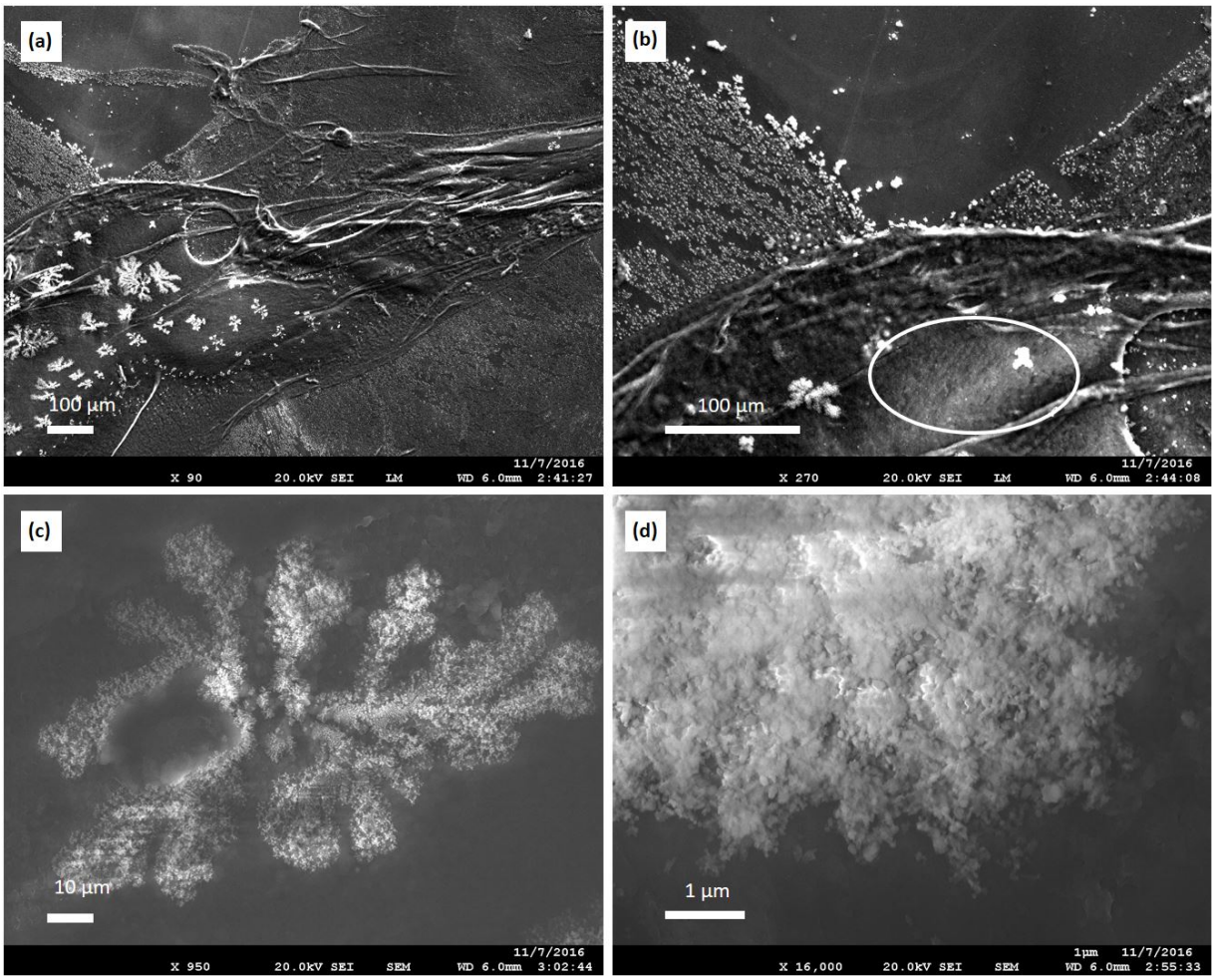

Figure 4.4: SEM images of sample $(Col/HyAp)(Col/HA)_2$ built within a templating PC membrane with an average diameter of 300 nm showing a consistent film coated by crystals (a), aligned tubular structures (white ellipse, b), a magnification of one of dendritic structure present on the film (c), a zoom on the previous structures showing cylindrical aggregated particles (d).

The fabrication of a film has been successfully done for the $(Col/HyAp)(Col/HA)_2$ system into PC membrane with pore diameter of 300 nm and is shown in Figure 4.4. The film looks resistant as it is quite folded (4.4 a). By magnifying the picture, the aligned tubular structures observed in the controls are also present (4.4 b). On the surface of the film, some cracked dendritic structures composed of small crystals are present (4.4 c). By looking closer to those structures, it appears that they are composed of small aggregated spherical particles (4.4 d).

Compared to the controls, large dendritic structures can be observed and are believed to be HyAp as it has never been observed before. The commercial HyAp has a needle shape, however in this case, the supposed HyAp has a spherical shape. On the other hand, HyAp is aggregated on the surface and not adsorbed on the collagen. The possibility that HyAp is adsorbed on collagen is not excluded but it is not likely to be the case. HyAp aggregates are larger than the pore diameter, showing that it aggregates after the release of the tubes. This demonstrates that HyAp was not well incorporated into the system, otherwise it would not have moved to create aggregates.

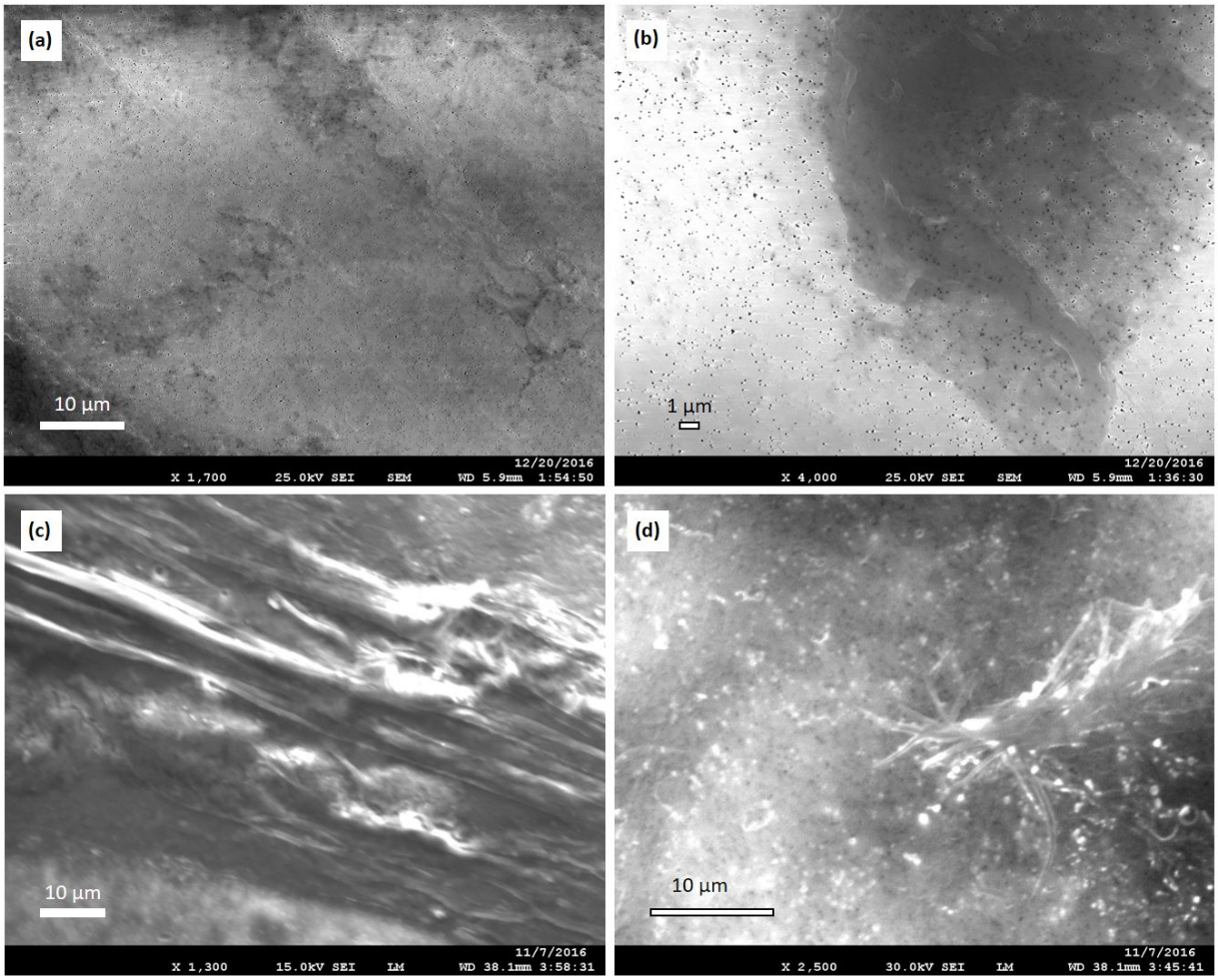

Figure 4.5: SEM images of sample $(Col/SiO_2)(Col/HA)_2$ showing some polymer bundles on the surface of the substrate (a) and a magnification on one of the polymer bundles (b). SEM images of the sample $(Col/HyAp)(Col/HA)_2$ are also presented showing a folded film (c) and tentacles shapes of polymer (d).Both samples were built within a templating PC membrane with an average pore diameter of 40 nm.

The results obtained with nanopores of 40 nm are presented in Figure 4.5. The build-up of the $(Col/SiO_2)(Col/HA)_2$ system leads to the formation of small polymer bundles dispersed on the surface of the substrate (4.5 a). The image magnification on one of those bundles (4.5 b) does not reveal any tubular shape or nanotubes. On the contrary, a film can be observed on the sample $(Col/HyAp)(Col/HA)_2$ (4.5 c)[2]. This film is quite folded, showing a certain solidity. Moreover, some parts of the film have a tentacle shape with a diameter approaching 300 nm (4.5 d). HyAp was not observed, however, the poor image quality of the $(Col/HyAp)(Col/HA)_2$ sample could prevent from seeing it.

[2]The images (4.5 c) and (4.5 d) have been taken in low magnification.

It is worth noting that the sample $(Col/SiO_2)(Col/HA)_2$ has been observed one month after the build-up. However, the sample was cross-linked and conserved within its supporting template. It was stored in the fridge, within a multi well plate filled with a 150 mM NaCl solution at pH 4. In those conditions, the sample should not have been degraded since its fabrication but this assumption cannot be demonstrated. Moreover, even if the sample was immersed for one month in the NaCl solution, no salt was observed. While in some other cases, a large amount of salt was present on the sample with a storage time of only two or three days.

The production of a film within pores of 40 nm in diameter is quite surprising. Indeed, due to the large size of the collagen molecule, this is unlikely that collagen can diffuse through the pores. Apparently, in those conditions, it has enough time to diffuse even in small pores. However, the film is discontinuous, unlike the case of the control. This suggests that collagen diffused more heterogeneously through the membrane.

Those three samples already evidence that the pore size has a great impact on the film formation. The film created into PC membranes of 300 nm are composed of tubular structures. Moreover, HyAp does not incorporate itself like the SiO_2 nanoparticles but form aggregates on the surface of the film. The morphology of the HyAp has also changed with the pH, from a needle shape to a more spherical one.

4.1.3 Influence of the pH on the aggregation of the commercial HyAp dispersion

As demonstrated previously in this chapter, at pH 4 HyAp is aggregated and does not incorporate itself into the nanotubes properly. In order to better understand this aggregation, the morphology of HyAp nanocrystals has been observed in its commercial form and at pH 4. Moreover, a DLS study has been performed to see in which conditions HyAp aggregates.

Commercial HyAp suspension

Commercial HyAp was first observed with SEM. For the observation, a drop of HyAp was deposited on a PET membrane coated by Cr and air dried for 4 days. The size of the HyAp needles were shown to correspond to the range of 20-50 nm, specified by the supplier (Figure 4.6 (a)). In this case, the size of the particles corresponds to its largest axis. The SEM images were not very clear and J. Landoulsi provided the TEM image (4.6 b) which has a better resolution. The size of the particles can be more easily measured and still corresponds to the supplier information.

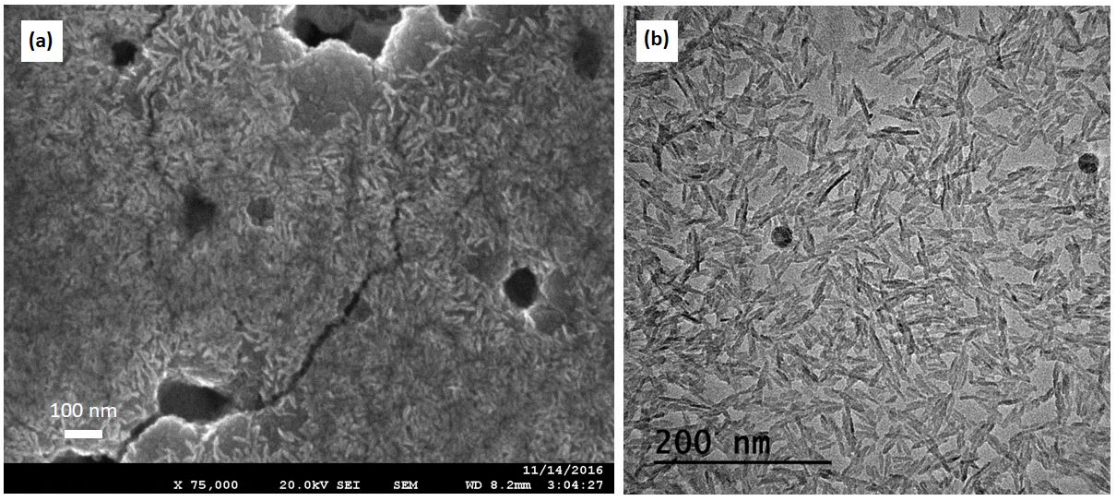

Figure 4.6: SEM (a) and TEM (b) images of commercially available HyAp.

To measure more precisely the size of the particles, a DLS experiment (Figure 4.7) has been performed on the commercial dispersion of HyAp (4.7 a). Moreover, to check the effect of the dilution, the size of HyAp diluted in Mili-Q water at 0.1% (4.7 b) and 0.01% (v/v) (data not shown) was measured.

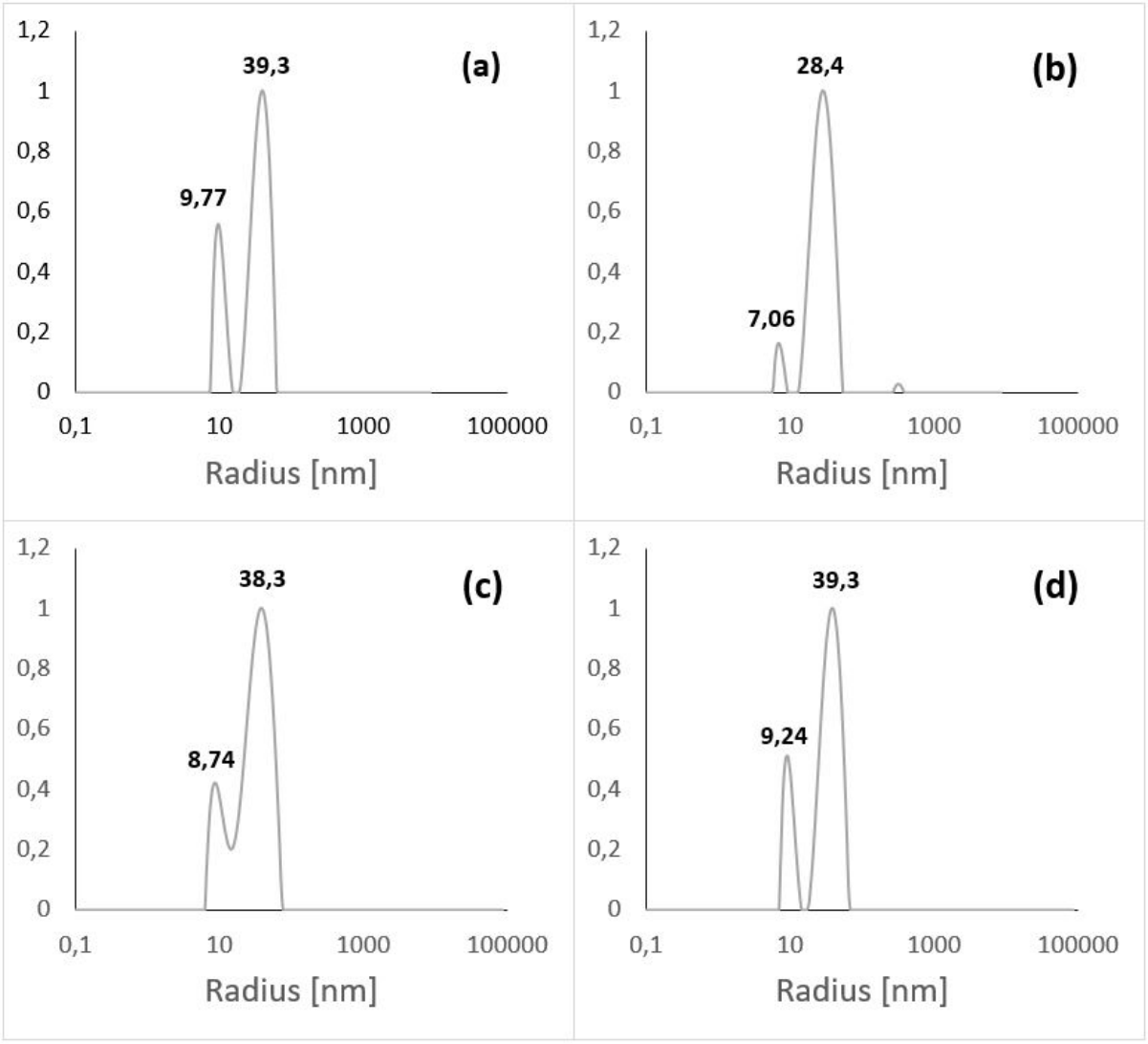

Figure 4.7: DLS measurement of commercial HyAp (a), diluted to 0.1 % (v/v) (b), filtered through a PC membrane with intersected pore of 300 nm (c) and through the same membrane with one layer of collagen (d).

The effects due to the filtration were also investigated. The commercial suspension of HyAp was filtered through PC membrane with intersected nanopores of 300 nm (4.7 c). HyAp was also filtered through the same membrane coated with one layer of collagen (4.7 d). The DLS was done on the suspensions recovered after filtration. By this experiment, the effect of filtration on the HyAp can be observed. Moreover, during the passage of HyAp (being at pH 9) through the pores, the local pH increases and could affect the collagen. If the collagen was desorbed during this step, some of it should be in the collected solution and would be observed on the DLS curve.

The four curves of Figure 4.7 are very similar. Two peaks can be observed, one around 10 nm and another around 40 nm. The only difference observed is a smaller second peak at 28.4 nm and a small peak between 100 and 1000 nm for the HyAp at 0.1%. The results of HyAp at 0.01% are not shown as the concentration is too low to obtain interpretable results.

The size measured for natural HyAp is slightly different from the one provided by the supplier. This can come from the instrument or from the supplier. The given information are not always perfectly exact. In any case, the difference is minimal and it has no adverse effect for the experiments.

The presence of two peaks usually corresponds to two different populations. However, it is likely to believe that those two peaks are due to instrumental issues. Moreover the particle geometry is anisotrope which can be more difficult to characterize. Based on the SEM and TEM images and the information of the supplier, it is more likely to believe that those two peaks reflect a more dispersed distribution of radii between 9 and 40 nm.

In the case of this work, the exact size of the HyAp particles is not necessarily needed, having a rough idea of it is sufficient. However, the characterization of HyAp in its commercial form is of great importance, to further determine whether it tends to aggregate.

The effect of dilution does not show a great impact on the particle size. The two curves (4.7 a) and (4.7 b) corresponding to natural and 0.1 % diluted HyAp respectively are similar. The shift in the particle size can be considered as minimal and the small peak between 100 and 1000 nm on (4.7 b) is due to some dust in the solution. The filtration does not affect the particle size as curves (4.7 c) and (4.7 d) are similar to the one of pure HyAp. Moreover, the filtration does not seem to desorb collagen from the PC membrane as no peak around 300 nm (the size of the collagen molecule) can be seen. However, the local increase of pH in the nanopores can still affect the collagen, by changing its surface charge for example but DLS does not allow to highlight such effects.

HyAp 1 % (v/v) at pH 4

To observe this sample, a drop of the HyAp solution was deposited on a PET surface coated by Cr. The SEM images obtained are shown in Figure 4.8 where HyAp aggregates can be clearly spotted (4.8 a). It forms a mat, however, it was not spread all over the surface. Only a part of it was covered by the HyAp mat. By looking closer on the HyAp, the aggregate is composed of HyAp in its needle shape forming a kind of porous mat (4.8 b).

Those images confirm that HyAp aggregates at pH 4 and that the aggregates observed in the previous part of this chapter (Figure 4.4 d) was well HyAp. However, it appears that HyAp does not aggregate in the same way. Previously, the aggregates formed a dense bundle made of small beads while in this case, it forms a mat composed of aggregated needles.

This difference can be explained by the presence of several species such as collagen and HA or the salt from the polyelectrolytes and the rinsing solutions. Moreover, HyAp in the intersected systems was filtered, the pressure applied during this step may influence its structure but no information about the effect of the pressure could be found in the literature. However, interactions between collagen and HyAp have been widely investigated. In the work of Tampeiri et al. [34] needles of HyAp have been observed on collagen fibers. This shows that collagen does not affect the structure of HyAp. The interactions between HyAp and HA have not been investigated yet but there is no reason to believe that HA influences HyAp in such a way. It is more likely to believe that this effect is due to the presence of salt. At this pH, the higher ionic strength may influence the transition of needle shaped HyAp towards a more spherical structure.

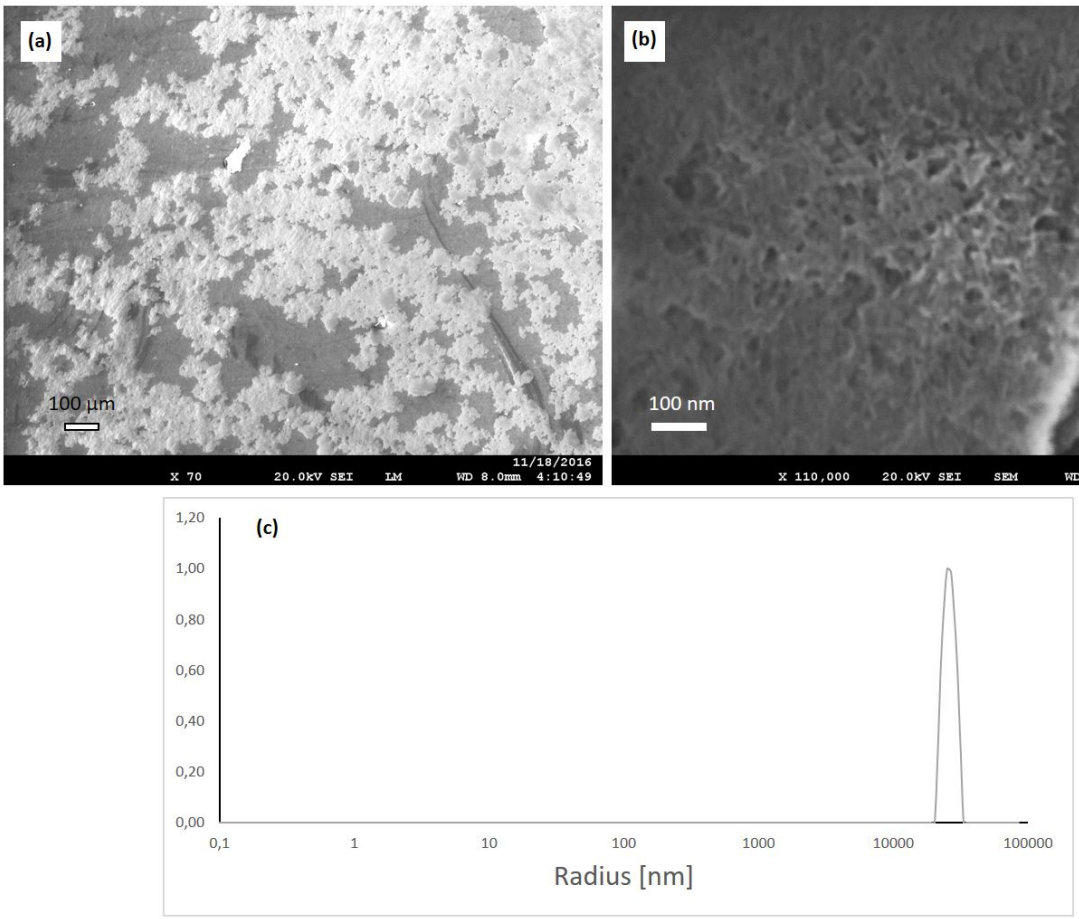

Figure 4.8: SEM images of commercial HyAp 1% (v/v) at pH 4 on PET substrate coated by Cr (a) and magnification on the aggregated HyAp (b). And the associated DLS measurement of this suspension (c).

CH_2Cl_2 has no significant effect on HyAp. Indeed, it can dissolve some organic compounds but it is not likely to interact with the HyAp which is inorganic. Moreover, CH_2Cl_2 is a polar molecule but HyAp is diluted into water with a higher dipolar moment. Then its polarity does not affect HyAp.

The results obtain by DLS for HyAp at pH 4 are undoubtedly different than for natural HyAp. Only one peak is obtained at more than 10 μm. This size is out of the range for the instrument and the exact particle size cannot be defined but it clearly shows that HyAp is aggregated.

Based on those results, a model explaining the different morphologies observed for the $(Col/HyAp)(Col/HA)_2$ can be proposed. During the filtration step, HyAp aggregates are too large to enter the pore of 40 nm. However, thanks to the pressure applied, the aggregates are fragmented and some of them can enter the pores of 300 nm. Those fragments are "trapped" in the tube but they are still too large to be well incorporated to the nanotubes. During the releasing step, the fragments of HyAp aggregates are freed and can reassemble onto the film of collagen and hyaluronic acid. They reassemble in a kind of crystallization which could explain the dendritic structures. During the drying step, the film can contract or expand leading to local strains on the deposited HyAp making it crack. However, this is only one possible interpretation of the results, more experiments are needed to prove it.

Influence of various parameters on HyAp aggregation

In this section, different parameters have been investigated to highlight their specific influence on the aggregation of HyAp, such as the filtration step, a lower pH and the interaction with HA. Moreover, as HyAp starts to precipitate after a few minutes, both the precipitate and supernatant were analyzed. All the samples are derivatives of the solution of HyAp 1% (v/v) at pH 4 used in the previous section. The solutions were prepared the day before analysis and stored in the fridge overnight. A few minutes before the analysis, a part of the precipitate and the supernatant was collected. Just before the analysis, the samples have all precipitated and the solutions were manually stirred to homogenize the solution. The samples were observed with bare eyes before and after the DLS analysis to be sure that it had not yet precipitated. The filtration through nanopores of 40 nm was not investigated here because the films formed in this way are not as good as the ones created with the nanopores of 300 nm.

All samples preparations are resumed in the table 4.1 and the DLS results obtained for the different samples are presented in Figure 4.9.

Table 4.1: List of samples and their preparation for the DLS analysis.

Sample	Preparation
(a)	Dispersion recovered after filtration through PC membrane with pore diameter of 300 nm
(b)	Dispersion recovered after filtration through PC membrane with pore diameter of 300 nm coated with one layer of collagen
(c)	Recovered precipitate from the initial dispersion
(d)	Recovered supernatant from the initial dispersion
(e)	Solution at pH 3
(f)	Solution sonicated with HA

In the following description of DLS analysis, the peaks that correspond to a size smaller than the particle size (20-50 nm) are considered as being products of decomposition of HyAp. While the particles with a radius of 500 nm, ten times larger than the particles size are considered to be aggregated.

By comparing the solutions of commercial HyAp, after filtration through the PC membrane with (b) and without (a) collagen, it appears that HyAp is still aggregated in both samples as the peaks above 1 μm suggest. This also confirms that the aggregates can be fragmented to pass through the pores and reform after. Besides, as there are several peaks above 1 μm, this could suggest that different kinds of aggregates can be present in the solutions. Moreover, due to the absence of smaller peaks for sample (b), it is likely to believe that small HyAp can still incorporate into the system.

The analysis of the precipitate (c) also shows two peaks above 500 nm. This suggests again the possibility of two kinds of aggregations. However, the solution at pH 4 shows only one peak at more than 10^5 nm. This difference is quite surprising and is difficult to interpret. Indeed, as explained in the section 3.4, the signal of large particles is magnified compared to the one of smaller particles. The particles being more "dispersed" in the whole solution than in the precipitate, the signal of small particles should be less hidden.

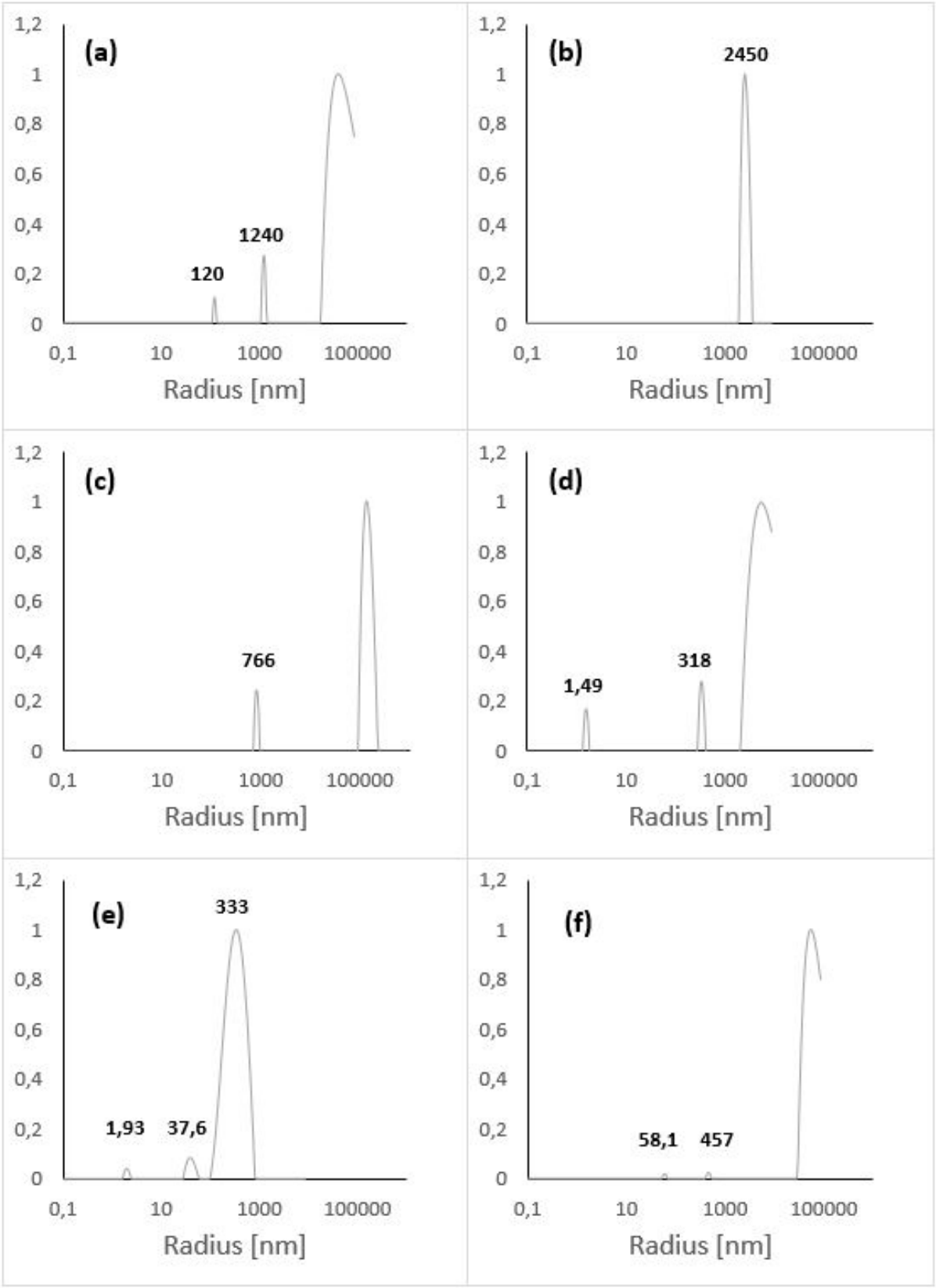

Figure 4.9: DLS measurement of HyAp at pH 4 filtered through PC membrane with pore of 300 nm (a), filtered through PC membrane with pore of 300 nm with one layer of collagen (b). DLS measurements of the precipitate (c) and the supernatant (d) both collected from the initial dispersion. HyAp at pH 3 (e) and HyAp at pH 4 sonicated with HA (f).

In the DLS curve of the supernatant, small particles can be observed because fewer larger particles are present. The peak at 1.49 nm shows that HyAp starts to be degraded at this pH. Some large aggregates are still present in the solution but in a lower concentration. This is proved by the presence of smaller peaks and also because the supernatant is transparent. The peak at 318 nm could represent the aggregation of only a few HyAp particles.

Before the analysis, the solution of HyAp which is usually milky looked perfectly clear at pH 3. This gave a first idea that a change in the solution occurred. Indeed, at this pH, HyAp is no more (or at least less) aggregated as no peak above 500 nm can be observed. Moreover, the smaller peak at 1.93 nm could reveal that a part of the HyAp decomposes itself. The peak at 37,6 nm is in the range of commercial HyAp. This could be interpreted as the result of the "desaggregation" of the HyAp or the non-aggregated HyAp that is no more hidden by the signal of the aggregates. However, if HyAp was not totally aggregated, this would have appeared in the DLS curve of the supernatant.

In the sample containing the HA, the large peak shows that HyAp is still aggregated. However, two much smaller peaks are also present and cannot be neglected. Indeed, their presence next to aggregates of more than 10^5 nm shows that those particles are present in a large amount.

To see whether one of the peaks corresponds to the HA molecules, its size in kDa must be converted into nm. This is possible by making some assumptions : HA is in random coil conformation and can be represented as a hard sphere and its mean density is 1.8 g/cm^3 [47]. With those assumptions, the molar mass in kDa can be related to the volume in nm^3 [48] :

$$M\ [Da] = \frac{6.023 \cdot 10^{23}\ [Da/g]\ \text{x}\ 1.80\ [g/cm^3]}{10^{21}\ [nm^3/cm^3]}\ \text{x}\ V\ [nm^3] = 1084.14\ V\ [Da]$$

Because the HA molecules can be considered as hard spheres the radius of one particle can be calculated :

$$R = \left(\frac{3V}{4\pi}\right)^{1/3} = 0.060 M^{1/3}$$

The molar mass of HA being between 151 kDa and 300 kDa, the radius of HA must vary between 3.51 and 4.42 nm.

However, those values do not appear on the DLS curve. Due to their small size compared to the HyAp aggregates of around 10^4 nm, it is not surprising that their signal is hidden. Based on those results, HA does not have much effect on HyAp which confirms the previous hypothesis.

In summary, HyAp can reaggregate after filtration through nanopores. Two types of aggregates have been observed, one around 1000 nm and another at more than 10^5 nm. However, this was not observed for unknown reason in the solution at pH 4. After the precipitation of HyAp, the majority of the large aggregates are in the precipitate while a minor part is present in the supernatant. HyAp is no more aggregated in the solution at pH 3 but it seems that HyAp start to be degraded and finally, HA does not seem to interact with the HyAp particles.

4.1.4 HyAp adsorption on HA instead of collagen

Due to the difficulty to incorporate HyAp nanocrystals to the collagen, the adsorption of HyAp on the HA layer instead of the Col layer has been investigated. Two $(Col/HA)(HyAp/HA)(Col/HA)_4$ samples were prepared with different HyAp concentrations: 1% and 0.1 % (v/v) in intersected nanopores of 300 nm diameter. The same method as for other experiments were used.

Figure 4.10 shows all the important features that could be observed on the sample containing 1% HyAp. On picture (4.10 a), the pores of the PET substrate (the black dots) can still be observed on the majority of the surface. By magnifying the image (4.10 b), a thin polymer layer can be observed. This layer is really thin and does not form a film made of tubular structures. However, in some places, tubular shapes forming a porous film can be spotted (4.10 c). Even by magnifying the image, HyAp could not be observed (4.10 d).

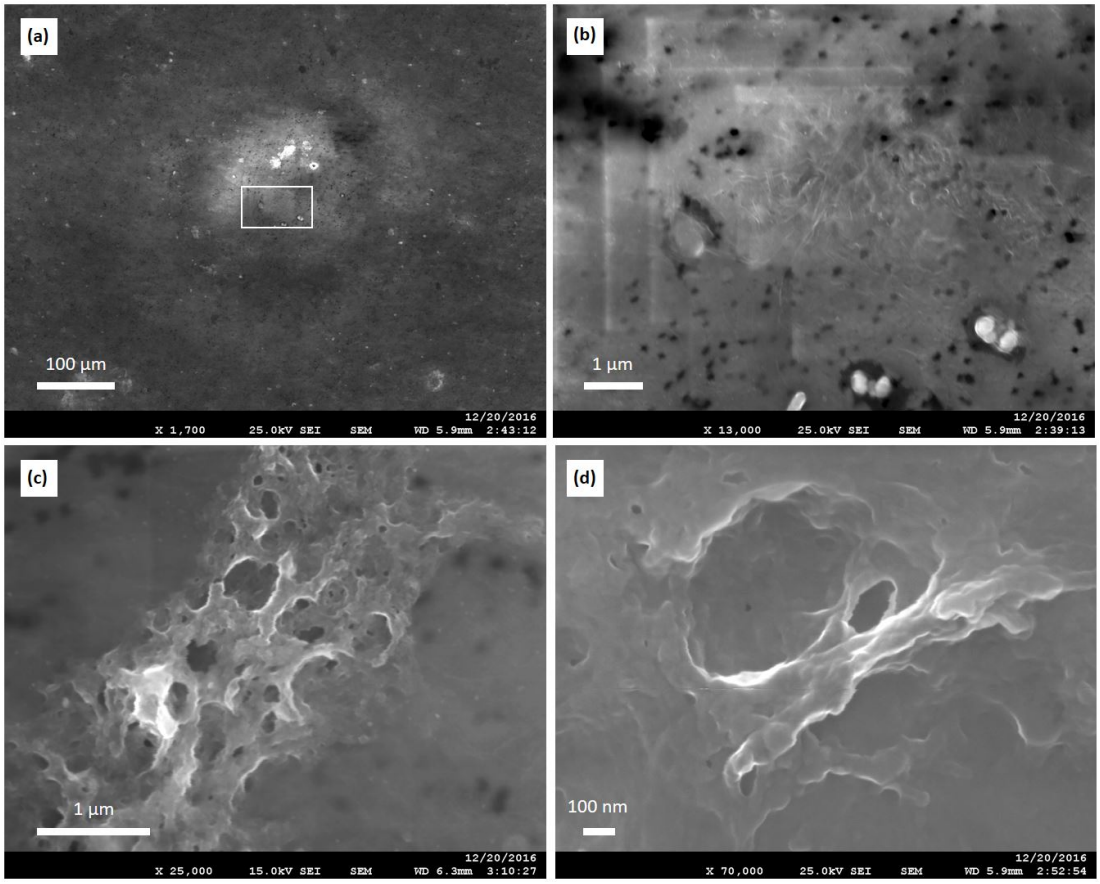

Figure 4.10: SEM images of the $(Col/HA)(HyAp/HA)(Col/HA)_4$ sample, prepared with HyAp 1% within PC membrane with intersected nanopores of 300 nm in diameter showing the PET surface coated by a thin layer of polymer (a), a magnification corresponding to the white rectangle showing a thin polymer film (b), the tubular structure of the film (c) and its magnification (d).

The SEM images of the sample created by the filtration of HyAp at a concentration of 0.1% (v/v) are presented in Figure 4.11. The synthesis of a consistent film has been well achieved (4.11 a). A part of the folded film is stratified and looks rolled up (4.11 b). The tubular shapes as in the controls can be observed (4.11 c). By magnifying those tubular structures, some protuberances can be seen (4.11 d).

By comparing the results of those two experiments, it appears clearly that the synthesis of nanotubes was better achieved at lower HyAp concentration. Indeed, in the sample with 1% (v/v) HyAp, the polymer mostly formed a thin layer on the PET substrate while in the case of 0.01% (v/v) HyAp, a consistent film is observed. In both cases, the system is collapsed as no intersected tubes could be observed. Moreover, even if tubular shapes could be observed, they were less organized than in the control which indicates a synthesis of lower quality.

The protuberances observed on the image (4.11 d) could be nanotube heads. However, by looking at the scale, their thickness does not correspond to the 300 nm expected. Their size being too thin to be nanotubes those protuberances could only be a part of the film which looks

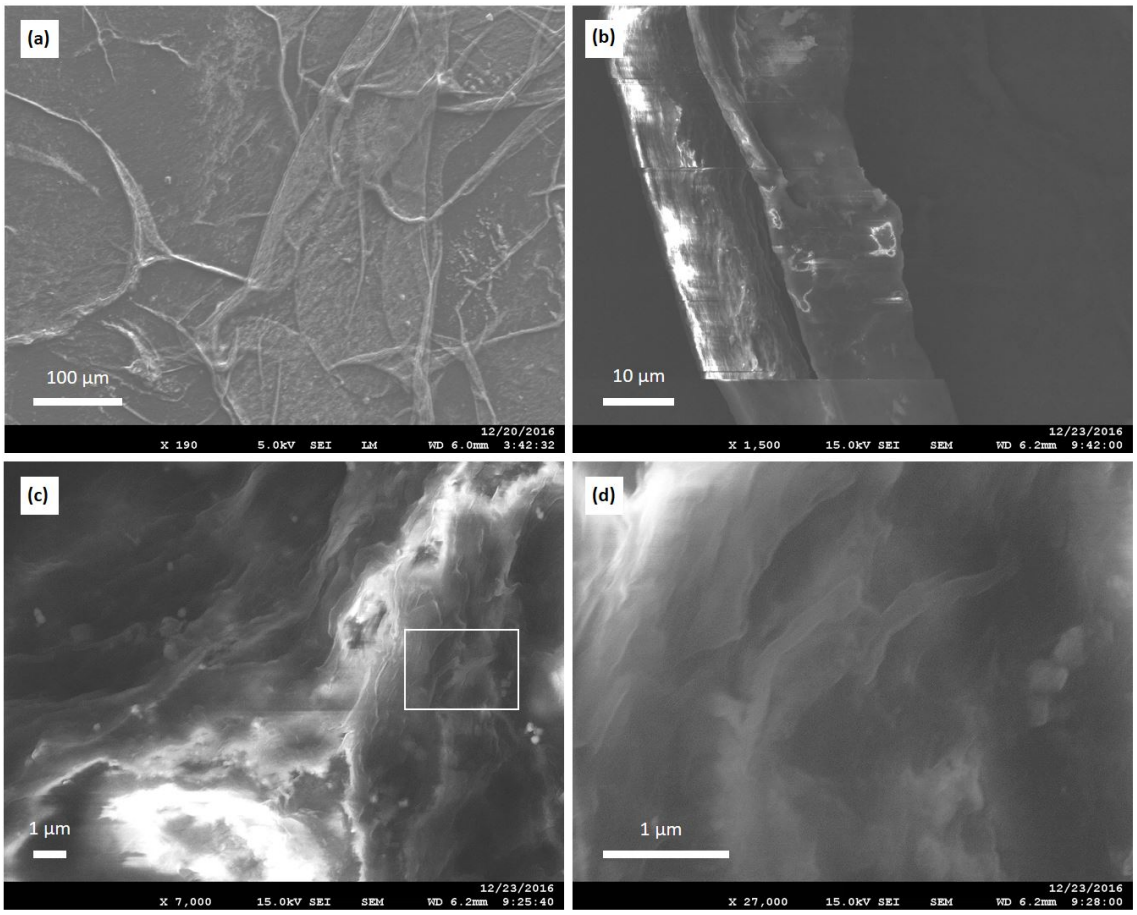

Figure 4.11: SEM image of (Col/HA)(HyAp/HA)$(Col/HA)_4$ sample, prepared with HyAp 0.1% within intersected nanopores of 300 nm diameter showing a consistent film (a), a part of the rolled-up film (b), tubular shapes of the film (c) and some protuberances on its side (d).

like nanotube heads. But the two structures appear to be very similar, the possibility that they are part of damaged nanotubes cannot be excluded.

HyAp could not be observed on those two samples. The adsorption of HyAp is again problematic, similarly as what was observed in the case of the filtration of the HyAp nanoparticles over a previously adsorbed collagen layer. However, by this experiment it appears that lower concentrations of HyAp lead to a better synthesis of nanotubes.

As a reminder, HyAp was purchased as a colloidal dispersion already in the nanocrystal shape. Its production and the composition of the solution in which HyAp is stored are not known. The components of the solution (such as additives added to avoid flocculation of the HyAp particles, surfactants,...) could prevent the formation of nanotubes. Moreover, those additives can be in solution but they can also be directly adsorbed on the HyAp particles. This could explain why less HyAp leads to a better film formation.

4.1.5 Replacement of HA by HyAp into collagen nanotubes

In this section, the different parameters investigated were the incorporation of HyAp as polyanion into the LbL system, the concentration of HyAp, the influence of the pH and the incorporation technique of HyAp. As the previous membranes were always collapsed, this study was made on simple tubes synthesized into PC membranes with parallel pore of 500 nm in diameter.

In this way, the influence of the different parameters could be observed more easily. The nanotubes synthesized by those methods were observed by SEM and the images collected are presented in Figure 4.12.

All the samples produced were of the type : $(Col/HyAp)_2/Col$, where HyAp was incorporated in the LbL build-up as a polyanion, therefore replacing the HA. In this way, HyAp was expected to adsorb on collagen and to form a negative layer to allow the collagen adsorption during the second deposition step.

To overcome the difficulty to incorporate HyAp, it was filtered twice through the system. This would increase the amount of HyAp adsorbed and the formation of simple rigid nanotubes was then expected.

The second parameter investigated was the concentration of HyAp. In the previous section, it appeared that less concentrated HyAp dispersion gave better results. Concentration of 0.01% (a,b), 0.1% (c,d,f) and 1% (e) (v/v) were investigated.

The influence of the pH on the nanotubes synthesis was also considered. The pH of the collagen, hyaluronic acid and rinsing solutions as well as the HyAp dispersion were fixed at pH 4 (a,c,e) and 5 (b,d,f).

Finally, two methods of incorporation of HyAp were tested. By filtration (a-e) and by immersion (f). Filtration of HyAp was done in the same way as the previously reported experiments. For the immersion, the membrane was dipped into the HyAp suspension for around 24 hours. During the immersion experiment, all solutions were fixed at pH 5 and HyAp suspension (at pH 5 also) had a concentration of either 0.1 % and 0.01% (v/v).

A summary of the different samples with their respective parameters is given in Table 4.2.

Table 4.2: Summary of the produced $(Col/HyAp)_2/Col$ systems along with their synthesis parameters.

$(Col/HyAp)_2/Col$	Concentration of HyAp			pH		Incorporation method	
	1%	0.1%	0.01%	4	5	Filtration	Immersion
(a)			X	X		X	
(b)			X		X	X	
(c)		X		X		X	
(d)		X			X	X	
(e)	X			X		X	
(f)		X			X		X
Not shown			X		X		X

By looking at the SEM images in Figure 4.12, nanotubes can be observed only when the synthesis was carried out at pH 4 with a HyAp concentration of 0.01% (4.12 a). Nanotubes were also observed for dispersions at pH 5 with HyAp concentrations of 0.01% (4.12 b) and 0.1% (4.12 d) and for the sample prepared by immersion (4.12 f). In all cases, the tubes are soft and their length is smaller than the thickness of the PC membrane (21 μm).

Polymer bundles were obtained for HyAp concentrations of 0.1% (4.12 c) and 1% (4.12 e) at pH 4. Those bundles have a tubular shape but look very huddled. In comparison with the previously described samples, they do not look like nanotubes. Concerning the sample with HyAp at a concentration of 0.01% at pH 5 made by immersion, no nanotubes, nor polymer bundles could be observed (results not shown).

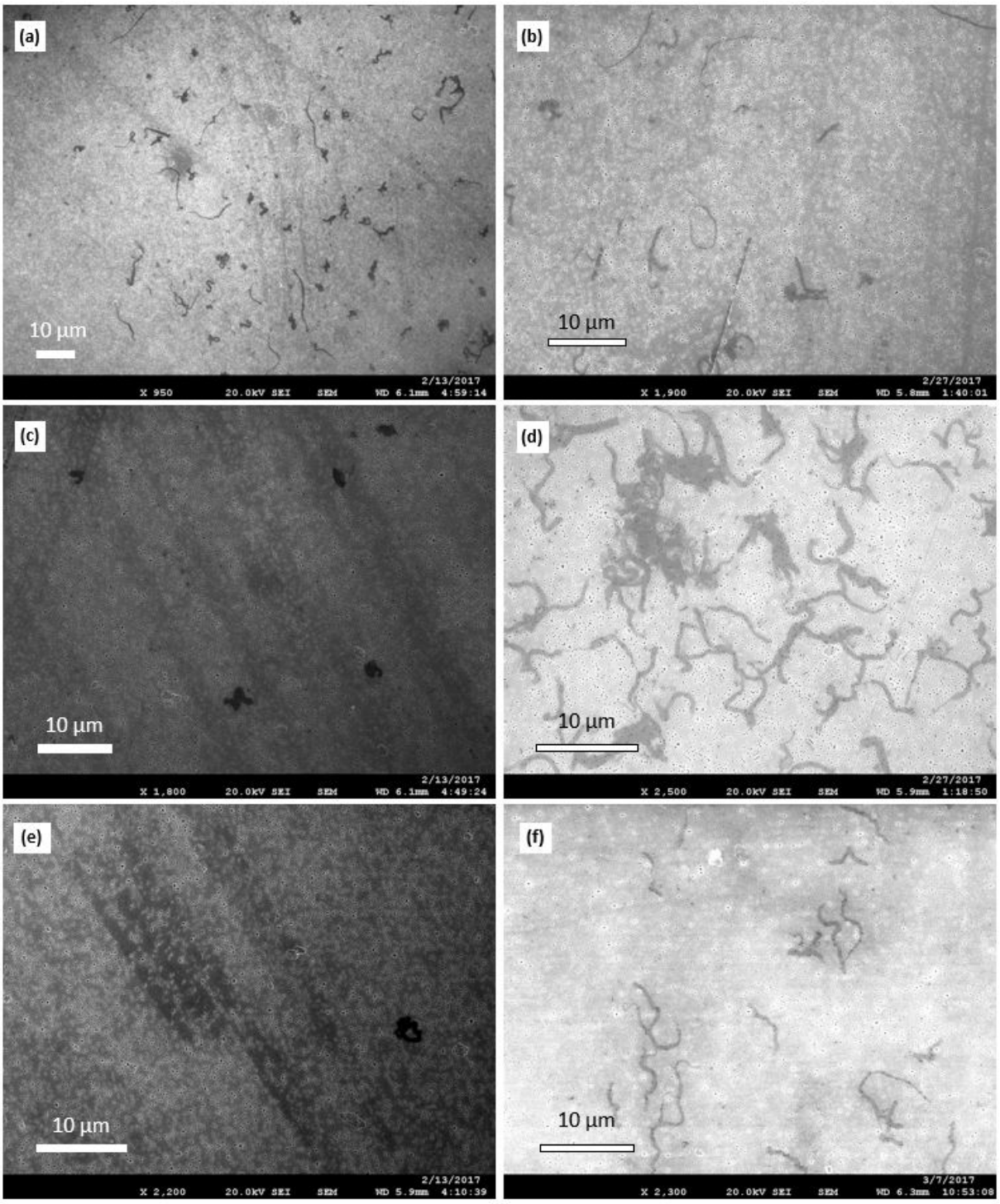

Figure 4.12: SEM images of simple $(Col/HyAp)_2/Col$ nanotubes synthesized at pH 4 for HyAp at a concentration of 0.01% (a), 0.1% (c), 1% (e) and at pH 5 for concentrations of 0.01% (b) and 0.1% (d) and by immersion for 24 hours into commercial HyAp dispersion at pH 5 (f).

Some trends come out of those experiments. The pH greatly influences the nanotubes synthesis, pH 5 appears to be more suitable than pH 4. The pH greatly influences the surface charge of weak polyelectrolytes. Collagen being a cationic polyelectrolyte, the lower the pH is compared to its isoelectric point (between 6 and 9.3), the greater is the charge of the molecule. Collagen at pH 4 should be more charged than at pH 5 and a better synthesis should occur. However, it has been reported that the pKa of adsorbed species could be different than the pKa

of the unadsorbed ones [11]. By comparison, if the isoelectric point of the collagen drops between pH of 4 and 5, the condition of the build-up are close to the isoelectric point which could explain the difference obtained during this experiment.

The concentration of HyAp also influences the nanotubes build-up. For nanotubes synthesized at pH 4, a decreasing concentration enhances the nanotubes formation. Nanotubes can be observed for HyAp at a concentration of 0.01% (4.12 a) but not for higher concentrations. This is in agreement with the results presented in the previous section. However, this trend is reversed for synthesis at pH 5. Indeed, in this case, it appears that higher HyAp concentrations lead to better tubes formations. This difference can hardly be explained but this experiment shows that the solvent of the commercial HyAp suspension does not prevent the nanotubes formation at pH 5 but it can still be the case for pH 4. However, such hypothesis cannot be confirmed with those experiments.

The filtration method also appears to be better than the immersion method. This should be due to the difficult diffusion of HyAp into the pore. During the filtration a larger amount of HyAp passes through the nanopores while a fewer amount passes during the diffusion.

The optimal conditions among the ones tested here, are HyAp at 0.1% (v/v) at a pH 5 filtered through the PC membrane (4.12 d). However, the tubes formed are still very soft and do not have a length of 21 μm. The softness and the magnification of the presented images (not shown) confirm that no HyAp was incorporated into the tubes. The nanotubes size, smaller than expected, shows that the tubes are damaged or only partially formed. The difficulty to incorporate HyAp nanocrystals to the systems is again encountered. To compensate for the poor incorporation of commercial HyAp, a new strategy, relying on the *in situ* nucleation of HyAp directly within the biomimetic systems, was elaborated.

4.2 *In situ* nucleation of HyAp onto biointerfaces of intersected $(Col/SiO_2)(Col/HA)_n$ nanotubes

In this section, different methods to incorporate HyAp by *in situ* nucleation onto ECM-like biointerface made of intersected nanotubes are proposed and compared. In the first part, the nucleation of HyAp into the tubes or outside them has been investigated. The second part focuses on different methods trying to prevent the intersected nanotubes from collapsing. Here, HyAp is used only for its biocompatible properties and not for its mechanical ones. Indeed, SiO_2 particles being easier to incorporate to the system and showing better results, this ceramic will be kept as rigidifying agent. The only role of HyAp will be to increase the biocompatibility of the biointerface.

4.2.1 Nucleation and characterization of HyAp particles

To investigate the feasibility of triggering the nucleation of HyAp by mixing $CaCl_2$ and NaH_2PO_4, the nucleation was first initiated in solution and the particles produced were collected on TEM grids to observe their morphology. The STEM images and the EDX analysis are shown in Figure 4.13. The STEM image (4.13 a) shows the needle shape of HyAp. However, due to the low quality of the image, it is not possible to determine the size of the particles. The EDX spectrum (4.13 b) shows two peaks at 2,013 and 3.690 keV which correspond to the K_α emissions of P and Ca, respectively. The other peaks show the presence of C, O, Cu, Na and Cl. It is worth noting that the EDX analysis is done on a square of 1 μm x 1 μm, the spectrum obtained is not precisely the one depicted on the STEM image but gives more an overall composition. This clearly confirms that the needles are composed of Ca and P. Nevertheless, it is difficult to state whether the particles produced actually consist in HyAp (with the chemical formula $Ca_5(PO_4)_3(OH)$) or simple Ca/P complexes. Indeed, the peak located at 0.6 keV that stands for the K_α emissions of

O can be due to the oxygen present in the HyAp but can also be due to the oxidation of the Cu substrate. In any case, for more simplicity, the term HyAp will be kept to refer to the particles nucleated *in situ*, even if they might not have the exact same chemical composition as native HyAp. The presence of the C is due to the carbon mesh covering the Cu-based TEM grid. While Na and Cl come from the calcifying solution. As a reminder, this solution is composed of $CaCl_2$ and NaH_2PO_4.

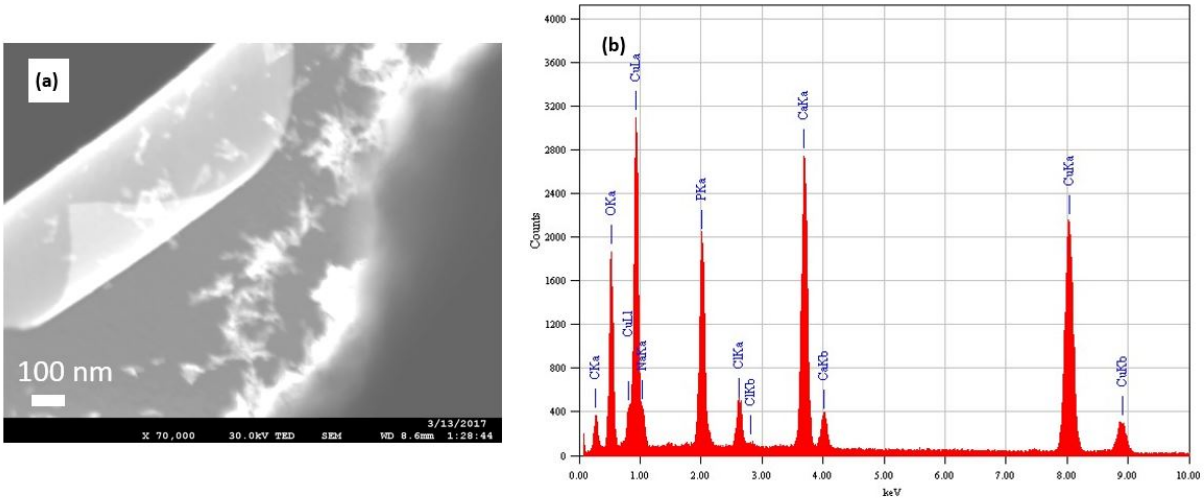

Figure 4.13: STEM image of HyAp nucleated *in situ* (a) and its EDX spectrum (b).

4.2.2 *In situ* nucleation of HyAp into individual nanotubes and onto intersected systems

The conditions in which the two systems are synthesized are quite different. For the incorporation into the tubes, the $(Col/HyAp)_2/Col$ system was produced at pH 5 into PC membranes with pores diameter of 500 nm. This experiment was done into simple tubes instead of intersected ones to be compared with the previous results. HyAp was deposited into this system by immersion of the sample into the calcifying solution during 24 hours at 37 °C.

For the *in situ* deposition of HyAp on the intersected system, the $(Col/SiO_2)(Col/HA)_2/HyAp$ was produced at pH 4 into PC membrane with intersected pores of 300 nm diameter. The HyAp deposition was done by immersion of the PC membrane into the calcifying solution for 24 hours at 37 °C after release and reticulation of the sample.

Those two systems were chosen as they previously gave the best results. The comparison of the two synthesis methods would show whether it is preferable to incorporate HyAp into individual nanotubes or onto the outer surface of the intersected nanotube systems.

In situ nucleation of HyAp nanoparticles within individual nanotubes

The STEM images of the incorporation of HyAp inside the tubes are presented in Figure (4.14). The EDX spectrum of this sample is not shown due to the small amount of collected nanotubes and the large minimal size of analyzed area by EDX (1 μm x 1 μm). The presence of HyAp would not be detected in any case, it would be lost in the signal of Cu and C coming from the TEM grid which are much more abundant. On this picture (4.14), two nanotubes can be

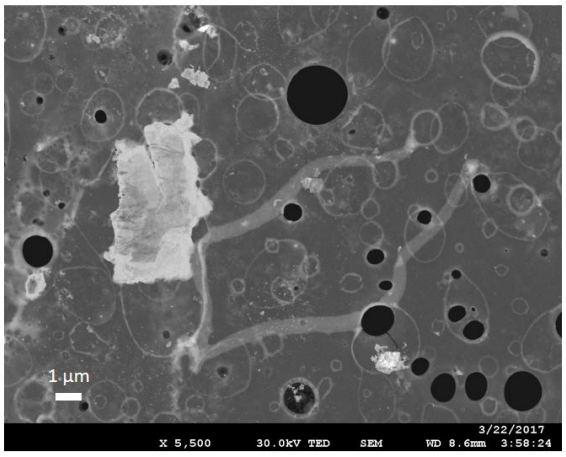

Figure 4.14: STEM image of the $(Col/HyAp)_2/Col$ system produced at pH 5 into PC membranes with pores diameter of 500 nm in which HyAp was nucleated *in situ* inside nanotube.

observed [3]. Their size corresponds approximately to the one expected, 21 μm long and 500 nm wide. However, the tubes look soft which suggests that HyAp was not incorporated correctly in the system. As explained before, this assumption cannot be proved. The kind of white rectangle in the middle left of the image (4.14) is an impurity of unknown nature.

In situ nucleation of HyAp nanoparticles onto a pre-existing biointerface

For the incorporation of HyAp outside the intersected $(Col/SiO_2)(Col/HA)_2/HyAp$ system, the SEM images are presented in Figure 4.15 and the EDX spectrum is shown in Figure 4.16.

On this sample, each component of the system could be observed separately and then altogether. Image (4.15 a) shows nanotubes head, (4.15 b) shows SiO_2 particles adsorbed on the nanotubes and (4.15 c) represents an area of the system covered by a layer of HyAp. The image (4.15 d) picks-up all the previously mentioned components in a single picture. The tubular structures can be observed, the SiO_2 can be seen on the top left part of the image and HyAp can be seen on the bottom right of the image.

On the EDX analysis made on an area with HyAp (4.16 a), the three main peaks are the ones of C, O and Si. Other peaks standing for P, Ca and Cr are also present. Finally, small peaks of Na and Cl can be observed. However, the analysis on an area without HyAp (4.16 b), used as negative control, show the peaks of C, O and Cr while there is no peak for the P and Ca. This confirms that HyAp was well nucleated onto the nanotubes. Moreover, even if a quantitative analysis was not conducted, SiO_2 clearly appears to be predominant, showing that SiO_2 is everywhere in the sample. The peak for carbon stands for the collagen and hyaluronic acid as they are mainly composed of carbon chains. The Ca and P peaks show that HyAp was well produced. The Cr peaks are due to the substrate which was coated by Cr before the SEM observations.

[3] They are attached at their extremity due to the merging of two pores into the PC matrix. This can happen as the ions irradiation used during the PC membrane fabrication is random.

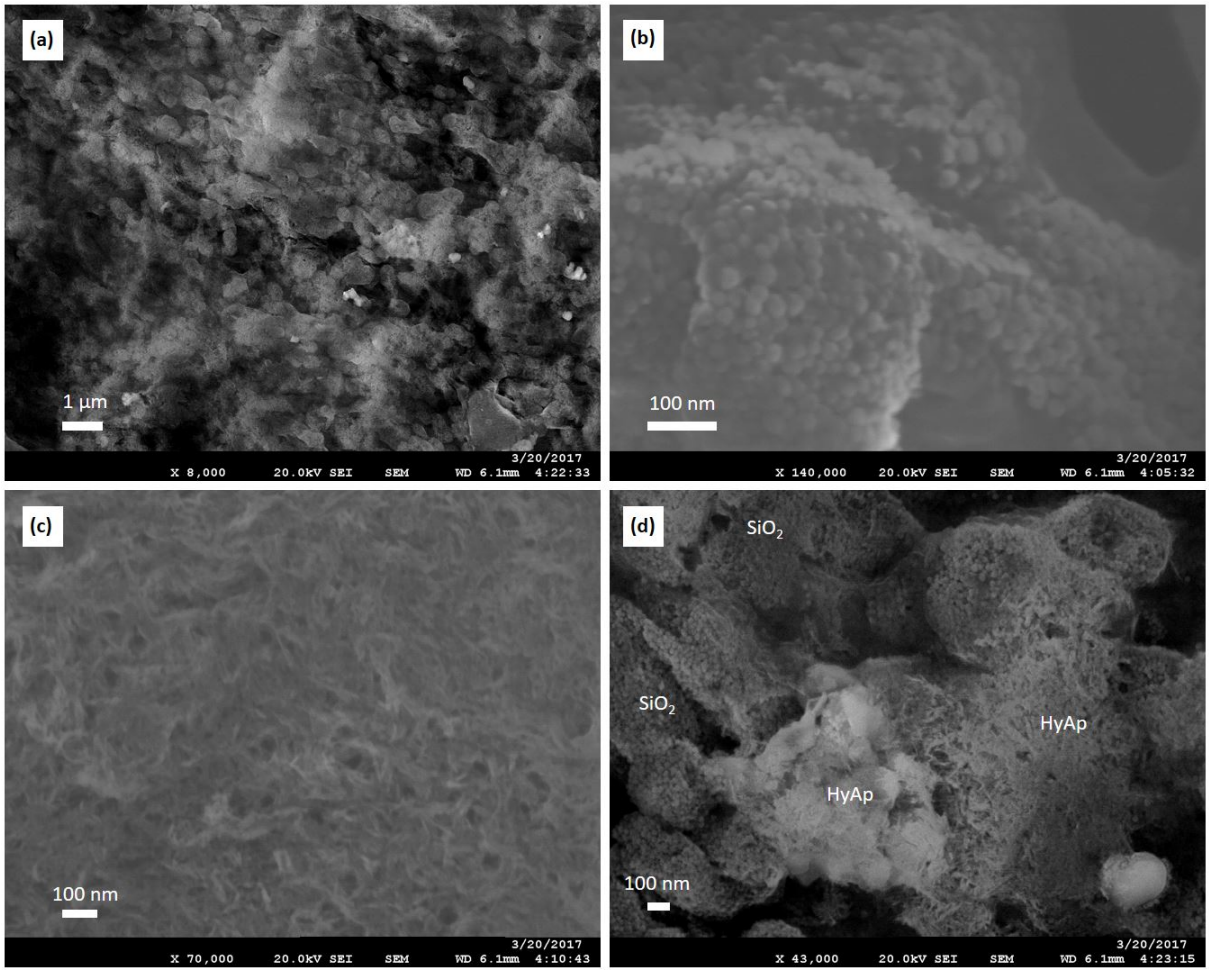

Figure 4.15: SEM images of $(Col/SiO_2)(Col/HA)_2$/HyAp systems in which HyAp was nucleated *in situ*, outside the intersected nanotubes, showing nanotube heads (a), SiO_2 particles (b), HyAp (c) and a global view of the system showing all the previously mentioned components (d).

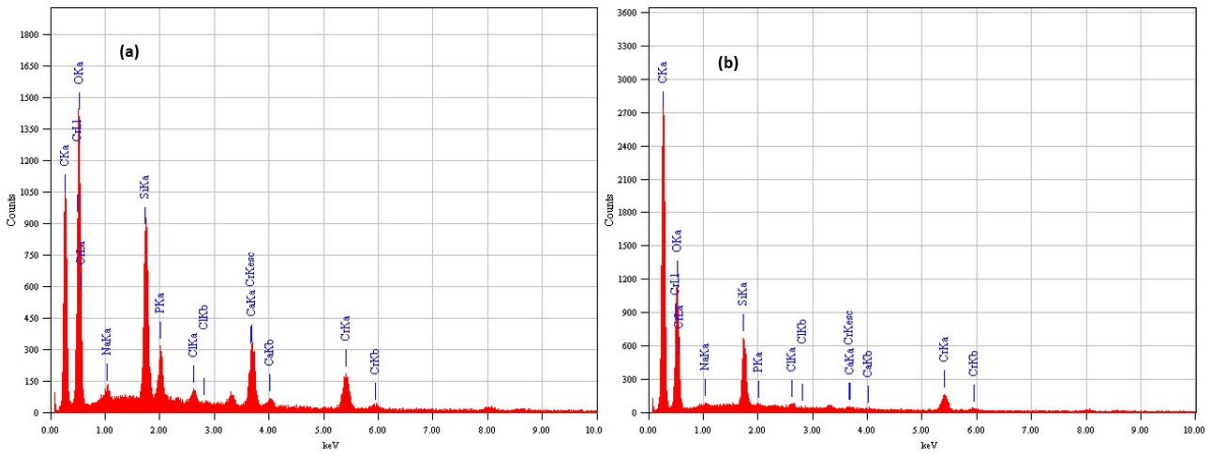

Figure 4.16: EDX spectra of $(Col/SiO_2)(Col/HA)_2$/HyAp system in which HyAp was nucleated *in situ* outside the intersected nanotubes. Analysis made on an area with HyAp (a) and without (b).

Those results show that HyAp was well incorporated to the system. Indeed, several areas are coated with HyAp. The produced film is then porous with tubular shapes coated by HyAp. However, this film is still composed of collapsed nanotubes, the thickness of the film is below 21 μm (image not shown). As explained before, this could be due to the PC membrane dissolution method or due to the pressure applied by the liquid on the freed sample during the immersion into the calcifying solution.

Moreover, by comparing the incorporation of HyAp in and out of the nanotubes, the last case shows better results. Indeed, the nanotubes were properly synthesized which was not the case when the nucleation was triggered within the nanotubes. In the case of *in situ* nucleation of HyAp onto a pre-existing biointerface, the system is reticulated before the nucleation step. The system is then more stable and the different effects of the temperature and pH affect less the system. This synthesis is then "easier" than the other one because less control is needed on the synthesis conditions.

The sample produced by *in situ* nucleation onto the system could be a good candidate for bone cell culture. Indeed, a porous biointerface made of tubular structures similar to the one of the ECM is well synthesized. Moreover, the presence of HyAp on this biointerface makes it more similar to the ECM of bone. However, a mechanically stable film is still not achieved. The next section will thus focus on finding a method to avoid the collapsing of the film.

4.2.3 Presentation of different methods attempting to avoid the collapsing of the biointerfaces

In the previous part, the hypothesis was made that the collapsing of the system was a consequence of the too high pressure applied on the system during the immersion into the solutions. In order to overcome that, two strategies were investigated : First, the number of Col/HA bilayers was increased in order to increase the wall thickness of the nanotubes and consequently, their mechanical strength. And second, the volume of the liquid during the immersion step is reduced in order to lower the pressure applied on the system.

Increasing the wall thickness of nanotubes

To increase the wall thickness of nanotubes, the numbers of bilayers was increased and the system $(Col/SiO_2)/(Col/HA)_5$/HyAp was produced. With this sample, an increase of the number of bilayers (resulting in an increase of the nanotubes thickness) was considered as a way to increase the mechanical strength of the system. This could prevent the system from collapsing during the immersion step but also during the release step. As the pH of the calcifying solution was fixed at 9, commercial HyAp was not likely to aggregate and samples with commercial HyAp and nucleated HyAp were synthesized to be compared. For the immersion step, the systems were dipped into commercial HyAp or into the calcifying solution (prepared as described in the Section 3.2) for 24 hours at 37°C and gently stirred.

The SEM images of the sample $(Col/SiO_2)(Col/HA)_5$/HyAp with nucleated HyAp are shown in Figure 4.17. The formation of a film was well produced (4.17 a). However, this film is quite folded. The SiO_2 that covers the nanotubes is also present (4.17 b) and intersected nanotubes are obtained (4.17 c). Those nanotubes also show a certain alignment, going from the bottom right corner to the top left one. Moreover, some bundles of HyAp are deposited on SiO_2 particles and thus on the nanotubes (4.17 d).

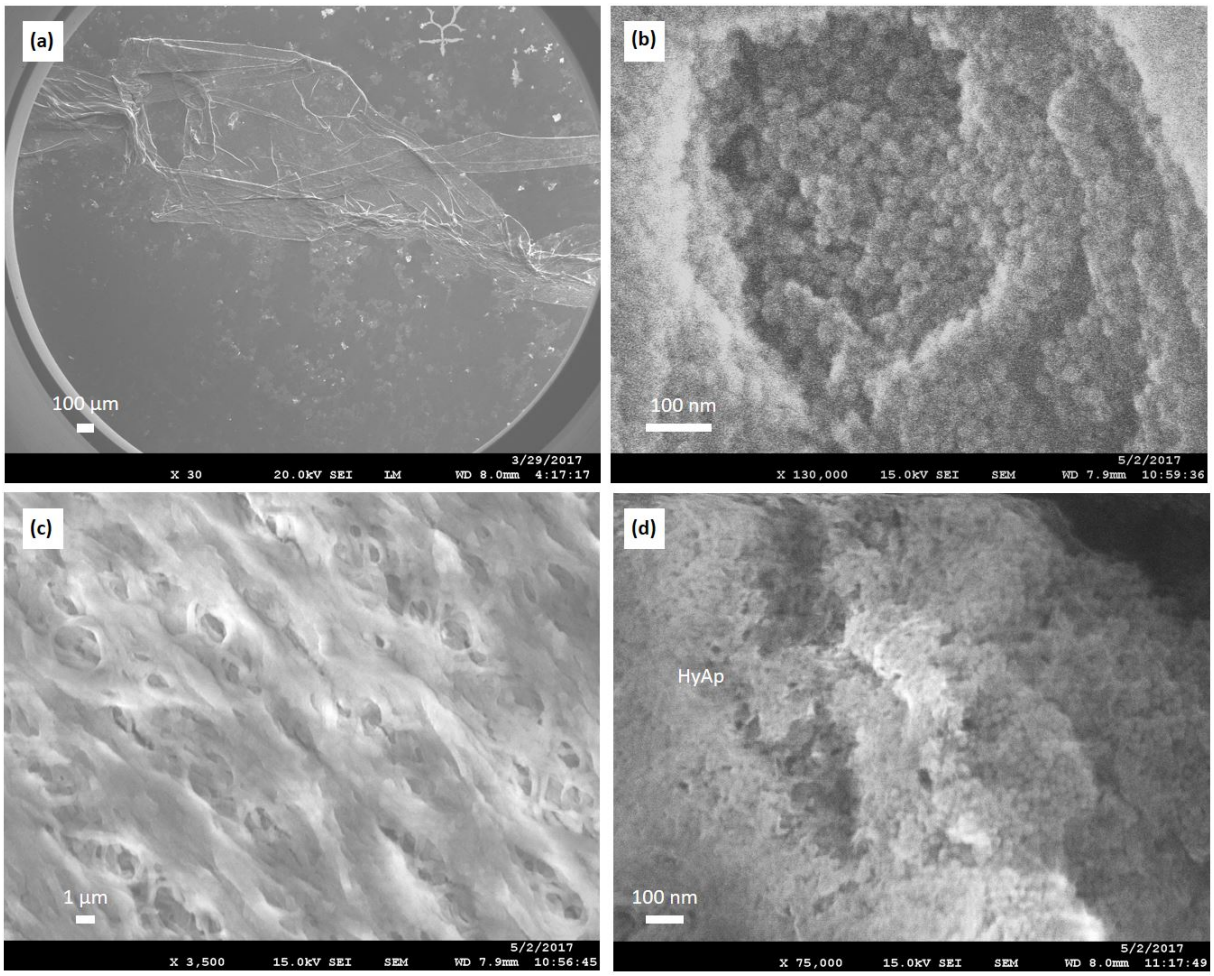

Figure 4.17: SEM images of $(Col/SiO_2)(Col/HA)_5$/HyAp system in which HyAp was nucleated *in situ* showing a folded resistant film (a), SiO_2 particles (b), intersected nanotubes (c) and HyAp (d).

Those images look very similar to the ones of the previous system (Figure 4.15). However, intersected nanotubes are more distinct in this case. Unfortunately, this kind of morphology where nanotubes are intersected but in the same time showing a kind of alignment is typical of collapsed systems. The reason of the collapsing of this system cannot be defined here, this could come from the releasing or the immersion step.

The SEM images obtained for the sample $(Col/SiO_2)(Col/HA)_5$/HyAp where HyAp was the commercial suspension are presented in Figure 4.18. Those images have a really low quality, the sample was charging much more than usual during the SEM observation and it was difficult to obtain images of good quality.

However, a folded film could be observed (4.18 a), on which the white areas on the film are due to the charging effect. Some SiO_2 particles and HyAp appear on a flat surface (4.18 b). Small bundles of HyAp can also be observed (4.18 c). They are deposited on a flat surface and form small spots that are very dispersed on the film.

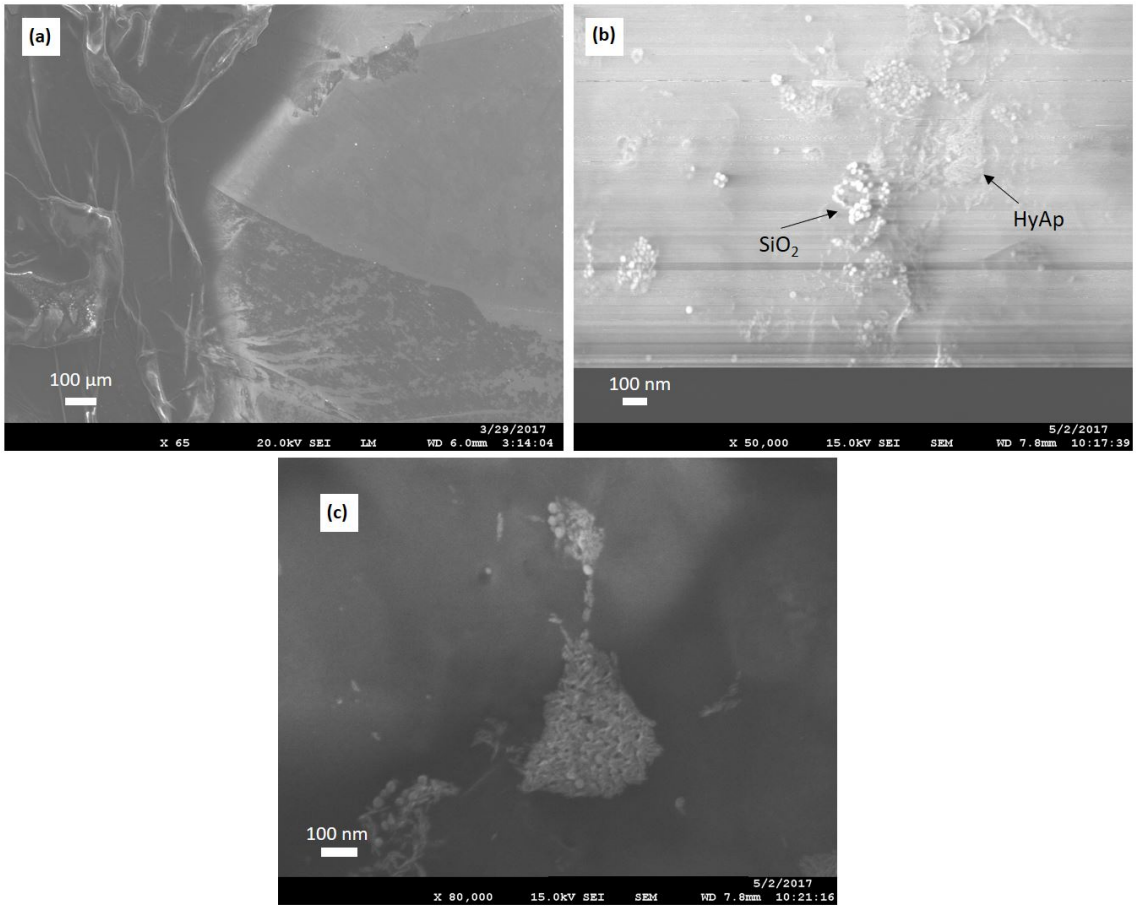

Figure 4.18: SEM images of $(Col/SiO_2)(Col/HA)_5$/HyAp system in which HyAp was the commercial suspension showing a folded film (a), SiO_2 particles and HyAp needles (b) and small HyAp bundles (c).

The results obtained on this sample are difficult to interpret due to the bad quality of the images. The flat surface that can be seen in Figure (4.18 b) and (4.18 c) is certainly an artifact due to the difficulty to obtain the images. The presence of SiO_2 particles on the flat surface suggests that it is composed of nanotubes. The reason why those particles can be observed in some place and not in others is supposed to be due to the roughness of the sample. Only the upper most areas could be seen due to a bad focus of the microscope.

Concerning the HyAp bundles, they were very dispersed on the film and they formed small spots. Those results are different than the *in situ* deposition where HyAp forms larger bundles located everywhere on the film. It was not possible to identify whether the sample was collapsed or not due to the poor image quality but the same conditions being used, it is likely to believe that it collapses.

The EDX spectrum of both samples are presented in Figure 4.19. In the spectrum of $(Col/SiO_2)(Col/HA)_5$/HyAp system in which HyAp was nucleated *in situ* (4.19 a), the SiO_2 signal is much larger than the other ones. To enhance the readability, a magnification of this spectrum was made (4.19 c).

This spectrum confirms what was observed by SEM. The peaks of Ca and P are present, even if they are partially hidden by the signal of SiO_2. The other peaks which stand for C, Na and Cl were also observed on the other samples.

On the spectrum of the sample coated by commercial HyAp (4.19 b), the same important peaks are present. It shows the presence of C, O, Si, P and Ca. The other peaks than Si and O are clearly seen as the signal of SiO_2 is less important in this case. Moreover, the peaks of Na and Cl are not presented but they are just side products and are not interesting in this work.

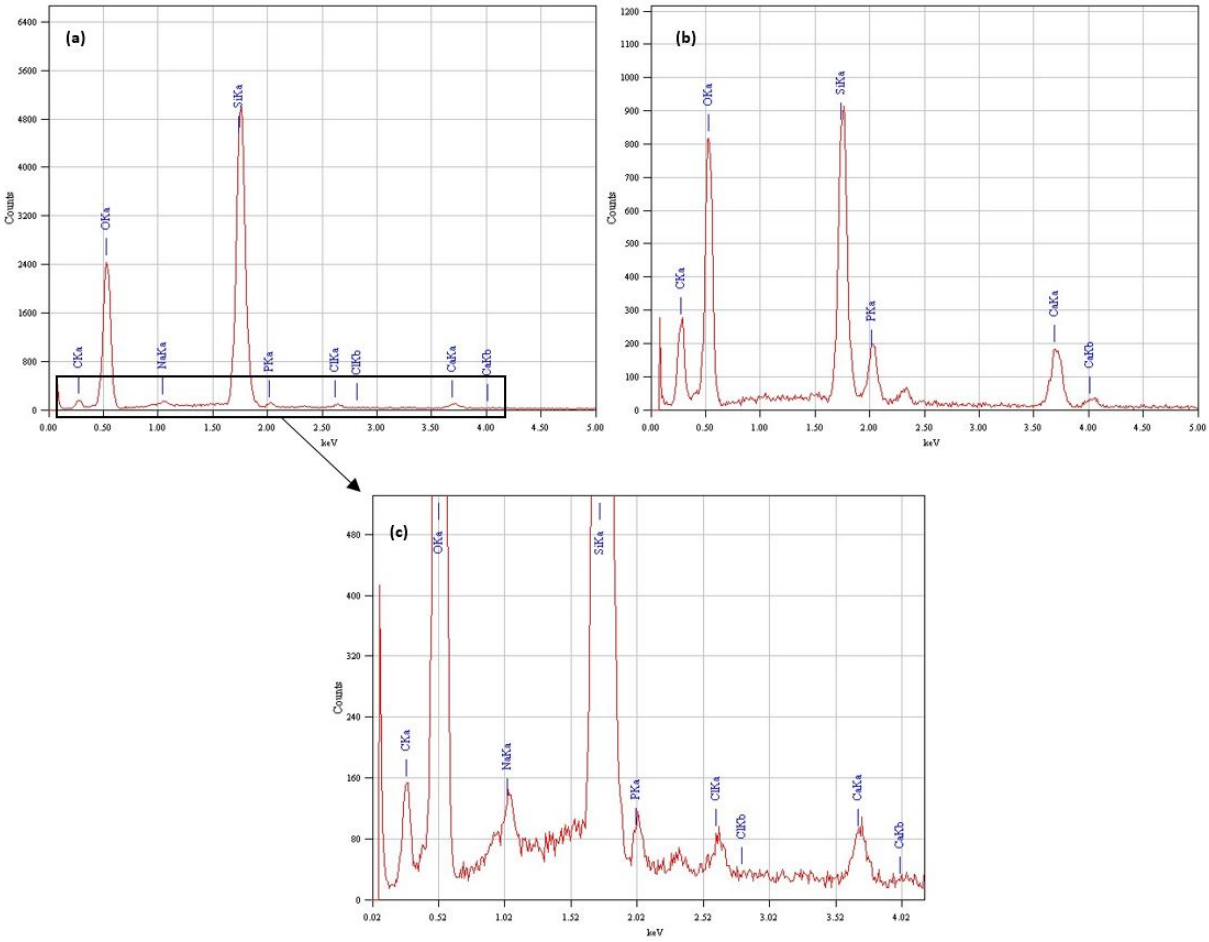

Figure 4.19: EDX spectra of $(Col/SiO_2)(Col/HA)_5$/HyAp system in which HyAp was nucleated *in situ* (a) and deposited from a commercial dispersion (b). A magnification of the first spectrum is also presented for more readability (c).

Those results show that six bilayers are still not enough for the system to be mechanically stable. However, it appears that HyAp deposited itself on the surface by forming bundles in the case of *in situ* nucleation as well as commercial HyAp deposition. However, nucleated HyAp creates more and larger bundles than the commercial one.

Lowering the pressure applied on the biointerface

As the sample sinks into the solution during the immersion into the calcifying solution, it is submitted to the pressure of the liquid above it. By reducing the solution volume and more specifically by reducing the volume/surface ratio, the pressure applied on the released system is lowered. In this way, the system is less likely to collapse during the nucleation step. However, the system still risks collapsing during the dissolution of the PC membrane by CH_2Cl_2.

For this experiment, the same $(Col/SiO_2)(Col/HA)_2$/HyAp sample as the one previously reported in this section has been synthesized. The only difference was that the immersion occurred into a multi well dish in which only 2 mL of the calcifying solution was poured. This

quantity was chosen to have enough HyAp while avoiding applying a too large pressure on the sample. Another sample, created in the same conditions excepted that it was immersed into the commercial HyAp instead of the calcifying solution was also produced. Due to instrumental issues, it was not possible to do the immersion step at 37°C. During the immersion into the calcifying solution, the pressure is believed to have a greater effect on the nanotube synthesis than the temperature. The immersion step then occurred at room temperature.

The SEM images of the sample immersed into 2 mL of the calcifying solution are presented in Figure 4.20. The focus on one edged of the film (4.20 a) shows that it is only a few μm thick, far from its expected value of 21 μm. This edge looks stratified and no intersected nanotubes can be observed. However they can be observed on the top of the film (4.20 b) showing a certain alignment, from the left to the right. HyAp is also present into the form of large bundles deposited on the surface of the nanotubes (4.20 c). Finally, on the last image nanotubes in the absence (top left) and presence (right side) of a HyAp crust (4.20 d) can be observed.

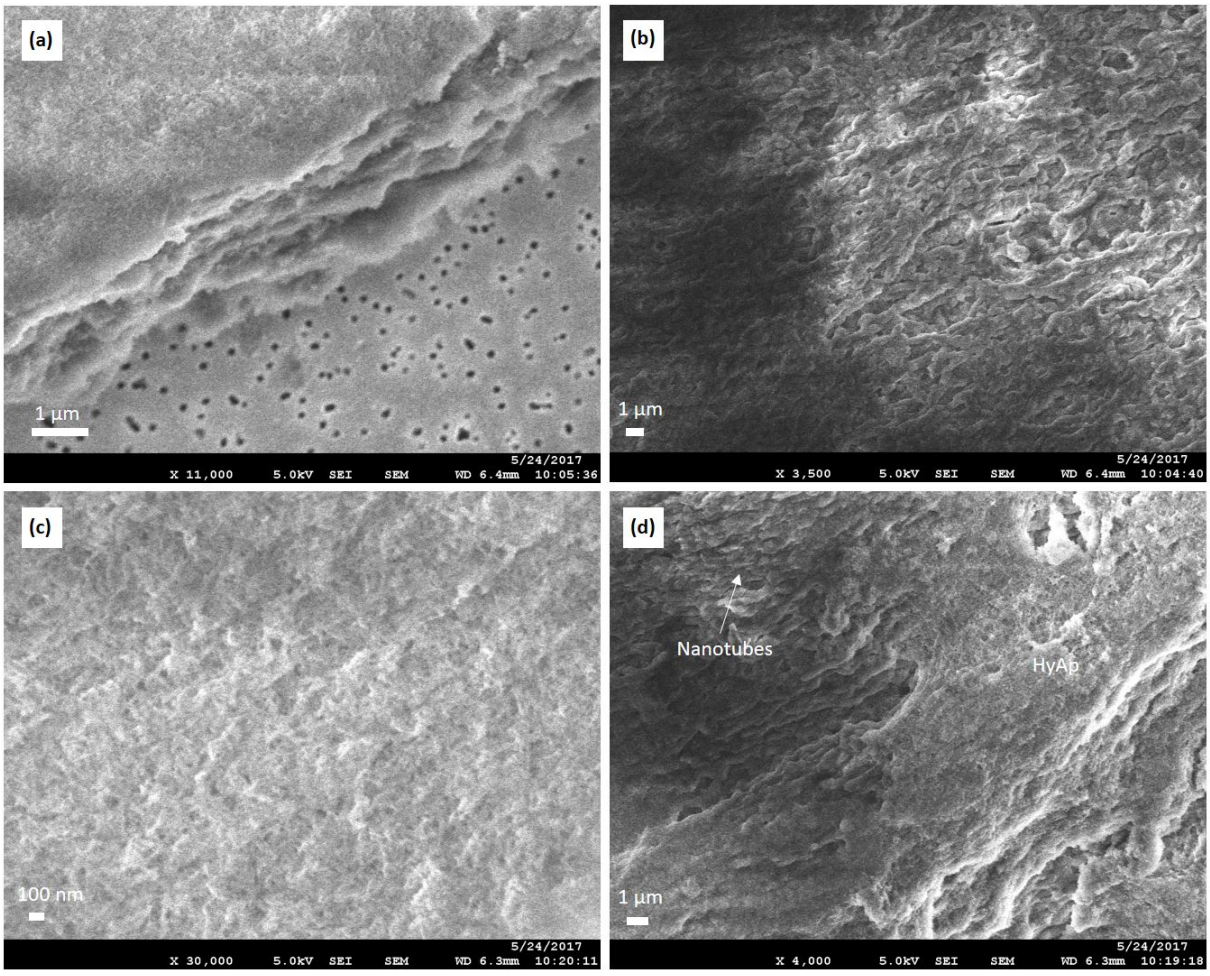

Figure 4.20: SEM images of $(Col/SiO_2)(Col/HA)_2$/HyAp system in which HyAp was dipped into 2 mL of the calcifying solution. Those images show a focus on the edge of the film (a), intersected nanotubes (b), HyAp (c) and nanotubes covered by HyAp (d).

The small thickness of the film edge shows that it is collapsed. This assumption is confirmed by the image showing the dense and aligned nanotubes on the surface of the film. HyAp is also present and still forms large bundles on the surface of the tubes. Those results are similar to the sample dipped into 10 mL of the calcifying solution. This could indicate than the collapsing

of the film occurs during the release step (i.e., when the PC template is dissolved) rather than during the nucleation/adsorption of HyAp. However, if it is already collapsed, the effect of the pressures applied can hardly be perceived.

The EDX spectra shown in Figure 4.21 highlight the differences that can be obtained by making the analysis at different places on the sample. The spectrum (4.21 a) was taken on a surface where only bare nanotubes were present. On this surface, no HyAp is present and the large peaks of Si and O are observed. On the contrary, when the analysis is done on surfaces where nanotubes are coated by HyAp (4.21 b), the signals of Si and O decrease and the peaks of P and Ca appear.

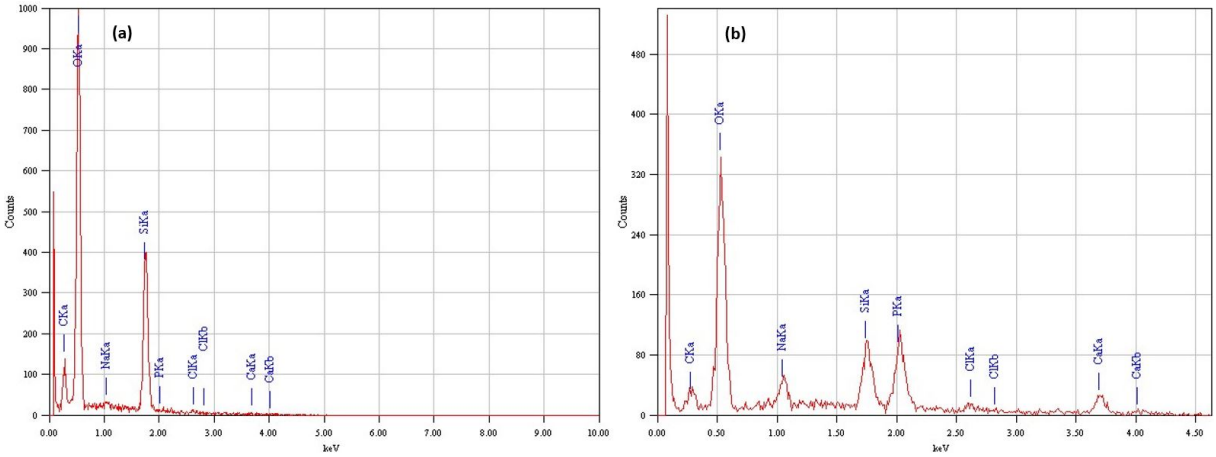

Figure 4.21: EDX spectra of $(Col/SiO_2)(Col/HA)_2$/HyAp system in which HyAp was dipped into 2 mL of the calcifying solution. The two spectra were taken from areas of bare nanotubes (a) and nanotubes covered by HyAp (b).

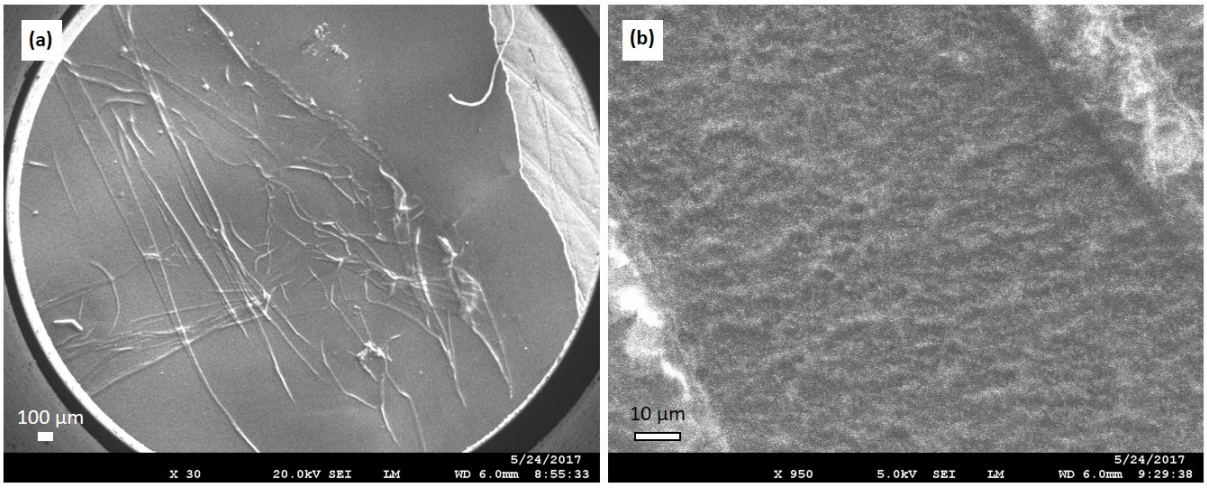

Figure 4.22: SEM images of $(Col/SiO_2)(Col/HA)_2$/HyAp system in which HyAp was dipped into 2 mL of the commercial HyAp suspension showing a film (a) with tubular structure on its surface (b).

The SEM images obtained for the sample dipped into 2 mL of the commercial HyAp (Figure 4.22) show a folded film (4.22 a) that reveals its resistance. By looking closer to the surface, some tubular shapes can be guessed (4.22 b). No other information could be taken from the SEM images of this sample. It is then impossible to see whether it is collapsed or not but regarding the previous results, it is likely to believe that it is collapsed.

In any case, those experiments show that HyAp was well incorporated to the systems when it was nucleated *in situ* outside the tubes. Indeed, as the sample is reticulated, the condition of nucleation, pH 9, do not disturb the adsorbed collagen nor change its surface charge distribution. However, it is not possible to determine whether HyAp is nucleated into the solution and then deposited onto the surface of the biointerface or if it directly nucleates on it. Despite several experiments, the film has always appeared to be collapsed. This could indicate that the collapsing occurs during the releasing step which was the only common step to the preparation of all samples.

Chapter 5

Conclusion and perspectives

The major goal of this thesis was to synthesize a biointerface that would mimic the ECM of bone to promote the adhesion, proliferation and differentiation of cells. Such a structure needs to be porous, made of tubular structures, mechanically stable and made of biological components. For this purpose, the mechanically stable system made of collagen and hyaluronic acid nanotubes with SiO_2 particles created by D. Lefèvre was taken as reference. The incorporation of HyAp in that system would increase the mechanical properties and its biocompatibility.

The first approach consisted in replacing the SiO_2 particles of the $(Col/SiO_2)/(Col/HA)_2$ system by nanocrystals of HyAp commercially available. HyAp was supposed to bring to the system the mechanical support it needed and also the biocompatibility. However, the HyAp was not well incorporated to the $(Col/HyAp)(Col/HA)_2$ system. Indeed, HyAp appeared to be aggregated on the surface of the film made of nanotubes.

Following those results, DLS experiments were conducted in order to better understand the aggregation of HyAp. It appeared that HyAp highly aggregates at pH 4 which was the pH at which all solutions were fixed. At this pH, the concentration of HyAp and the addition of HA to the dispersion did not seem to have an effect on the aggregation. However, two kinds of aggregations were observed, small aggregates between 500 and 3000 nm and large aggregates, larger than 10 μm. The presence of those aggregates after the filtration through the PC membranes with nanopores of 300 nm in diameter shows that the particles reaggregate after the filtration. Finally, at pH 3, HyAp is no more aggregated and a part of it is degraded.

Due to the difficulty to adsorb HyAp nanocrystals to the collagen, the adsorption of HyAp on the HA layer was investigated. It appeared that a less concentrated solution of HyAp for the build-up of the $(Col/HA)(HyAp/HA)(Col/HA)_4$ system gave results closer to the ones of the control. A film made of collapsed nanotubes was obtained for HyAp 0.1% (v/v) but not for 1%. However, the system was still collapsed and no HyAp could be observed.

The next approach to incorporate HyAp to the system was to replace the HA by HyAp to form $(Col/HyAp)_2/Col$ systems. In this case, the focus lied on the incorporation of HyAp into simple tubes with a diameter of 500 nm. Different conditions were investigated, the effect of the concentration (1%, 0.1% and 0.01% (v/v)), the pH (4 or 5) and the incorporation method (by filtration or immersion). It appeared that only nanotubes with bad morphology were obtained at pH 4 for concentration of 0.01% HyAp. At pH 5, nanotubes were obtained for all tested conditions, however, the best results were obtained for HyAp at 0.1% (v/v). It appeared that the filtration method was more suitable for the nanotubes synthesis than the immersion and HyAp was observed on none of those systems.

Incorporation of HyAp nanocrystals to the system appeared to be unsuccessful. Another strategy consisting in the *in situ* nucleation of HyAp on the system was investigated. Its

nucleation onto the $(Col/SiO_2)/(Col/HA)_2$ intersected system or into single $(Col/HyAp)_2/Col$ nanotubes were investigated. The results obtained showed that the *in situ* nucleation of HyAp onto the pre-existing biointerface was more adequate. Indeed, the SEM images and the EDX experiments showed that HyAp bundles were present on the surface of the nanotubes. In the case of HyAp incorporation into simple tubes, they appeared to be soft and no HyAp was observed in this system. By this experiment, the previous $(Col/SiO_2)/(Col/HA)_2$ system was made more biocompatible with the incorporation of HyAp. The mechanical properties are improved by the SiO_2 particles as the HyAp could not be successfully incorporated to the system. However, as for the previous experiments, the system was collapsed.

The goal of the last experiments was to prevent the collapsing of the biointerface. For this purpose, the number of Col/HA bilayers was increased and the volume of liquid during the nucleation of HyAp was lowered. In both cases, when HyAp was nucleated *in situ*, a film made of tubular structures covered in some places by HyAp were obtained. Those correspond to the previously reported results. The same experiments with the deposition of commercial HyAp nanocrystals could not be observed properly because the sample charged too much during SEM observations. In any case, for HyAp nucleated *in situ* or commercially available, the systems were collapsed. The synthesis of an ECM-like biointerface made of nanotubes composed of natural components was well achieved. However, the mechanical properties of the system still has to be improved.

All the produced samples showed a lack of mechanical properties. Several ways are still to be investigated in order to overcome this problem. As previously explained, the release step is very tricky. This step is suspected of being the cause of the collapsing of the systems. This experiment being manual, it would be interesting to make it more automatic. This could be done by using a drop-by-drop system in which the drops are deposited on the sample and do not fall on it. In this way, the quantity of CH_2Cl_2 and the time to pour it would be controlled, leading to a more homogeneous release of the system.

However, to check whether it is mandatory to obtain a mechanically stable structure, bone cell growth on the membrane could be investigated. Indeed, if the biointerface already shows to be a good environment for cells, it is then not necessary to improve its mechanical properties.

To improve the *in situ* nucleation of HyAp, different concentrations of $CaCl_2$ and NaH_2PO_4 in the calcifying solution could be investigated. Moreover, in the experiments described above, the nucleation of HyAp already occurs in the solution. To be sure that HyAp nucleated directly on the biointerface, the nucleation in three steps proposed by Yu [37] could be investigated. It consists in one activation step which creates negative sites. During the second step, the CaP induction, the sample is alternatively dipped into individual Ca and P solutions. This would produce the nucleation sites. The last step, called the mineralization, consists in dipping the system into simulated body fluid for 7 days. In this way, the HyAp is ensured to be nucleated onto the system and not into the solution before depositing itself on the biointerface.

The *in situ* nucleation of HyAp could also be done into nanotubes. This experiment may be difficult as the conditions inside the pores are not controllable with the available instruments. However, by creating a constant flow of the calcifying solution through the nanotubes and by gradually increasing the pH value up to 9, the HyAp nucleation inside the tubes might be possible. The incorporation of HyAp into the system could be done while it is still protected by the PC membrane. HyAp could be deposited at different places to create systems such as $((Col/HyAp)(Col/HA)_x)_n$ systems. Moreover, the HyAp incorporation could be done before or after the reticulation step. In this way, HyAp could replace the SiO_2 particles as it was first proposed. This would also allow to fully use the HyAp properties to improve the mechanical stability and the biocompatibility of the system.

Bibliography

[1] Francesco Rosso, Antonio Giordano, Manlio Barbarisi, and Alfonso Barbarisi. From cell–ecm interactions to tissue engineering. *Journal of cellular physiology*, 199(2):174–180, 2004.

[2] Jamil A. Matthews, Gary E. Wnek, David G. Simpson, and Gary L. Bowlin. Electrospinning of collagen nanofibers. *Biomacromolecules*, 3(2):232–238, 2002.

[3] Charles R. Martin. Nanomaterials : A membrane-based synthetic approach. *Science*, 266(5193):1961–1966, 1994.

[4] Veronica M. Cepak and C. R. Martin. Preparation of polymeric micro- and nanostructures using a template-based deposition method. *Chemistry of Materials*, 11(5):1363–1367, 1999.

[5] Yajun Wang, Alexandra S. Angelatos, and Frank Caruso. Template synthesis of nanostructured materials via layer-by-layer assembly. *Chemistry of Materials*, 20(3):848–858, 2008.

[6] Omar Azzaroni and Aaron K. H. Lau. Layer-by-layer assemblies in nanoporous templates: nano-organized design and applications of soft nanotechnology. *Soft Matter*, 7(19):8709–8724, 2011.

[7] Zhiyong Tang, Ying Wang, Paul Podsiadlo, and Nicholas A. Kotov. Biomedical applications of layer-by-layer assembly: From biomimetics to tissue engineering. *Advanced Materials*, 18(24):3203–3224, 2006.

[8] Halima Alem, Françoise Blondeau, Karine Glinel, Sophie Demoustier-Champagne, and Alain M. Jonas. Layer-by-layer assembly of polyelectrolytes in nanopores. *Macromolecules*, 40(9):3366–3372, 2007.

[9] Catherine Picart. Polyelectrolyte multilayer films: From physico-chemical properties to the control of cellular processes. *Current Medicinal Chemistry*, 15(7):685–697, 2008.

[10] Jan A. Johansson, Tobias Halthur, Merja Herranen, Lennart Söderberg, Ulla Elofsson, and Jöns Hilborn. Build-up of collagen and hyaluronic acid polyelectrolyte multilayers. *Biomacrmolecules*, 6(3):1353–1359, 2005.

[11] Pieter Bieker and Monika Schönhoff. Linear and exponential growth regimes of multilayers of weak polyelectrolytes in dependence on ph. *Macromolecules*, 43(11):5052–5059, 2010.

[12] C. Picart, J. Mutterer, Richert L., Y. Luo, G. D. Prestwich, P. Schaaf, J.-C. Voegel, and P. Lavalle. Molecular basis for the explanation of the exponential growth of polyelectrolyte multilayers. *Proceedings of the National Academy of Sciences*, 99(20):12531–12535, 2002.

[13] C. J. Roy, C. Dupont-Gillain, S. Demoustier-Champagne, A. M. Jonas, and J. Landoulsi. Growth mechanism of confined polyelectrolyte multilayers in nanoporous templates. *Langmuir*, 26(5):3350–3355, 2010.

[14] Wolfgang Friess. Collagen – biomaterial for drug delivery. *European Journal of Pharmaceutics and Biopharmaceutics*, 45(2):113–136, 1998.

[15] Jean Charvolin and Jean-François Sadoc. About collagen, a tribute to yves bouligand. *Interface Focus*, 2(5):567–574, 2012.

[16] Matthew D. Shoulders and Ronald T. Raines. Collagen structure and stability. *Annual review of biochemistry*, 78(1):929–958, 2009.

[17] Carole E. Schanté, Guy Zuber, Corinne Herlin, and Thierry F. Vandamme. Chemical modifications of hyaluronic acid for the synthesis of derivatives for a broad range of biomedical applications. *Carbohydrate Polymers*, 85(3):469–489, 2011.

[18] John A. M. Ramshaw, Yong Y. Peng, Veronica Glattauer, and Jerome A. Werkmeister. Collagens as biomaterials. *Journal of Materials Science: Materials in Medicine*, 20(1):S3–S8, 2009.

[19] Ana Marina Ferreira, Piergiorgio Gentile, Valeria Chiono, and Gianluca Ciardelli. Collagen for bone tissue regeneration. *Acta Biomaterialia*, 8(9):3191–3200, 2012.

[20] Wenguo Cui, Xiaohong Li, Chengying Xie, Huihui Zhuang, Shaobing Zhou, and Jie Weng. Hydroxyapatite nucleation and growth mechanism on electrospun fibers functionalized with different chemical groups and their combinations. *Biomaterials*, 31(17):4620–4629, 2010.

[21] J. R. E. Fraser, T. C. Laurent, and U. B. G. LAURENT. Hyaluronan: its nature, distribution, functions and turnover. *Journal of Internal Medicine*, 242(1):27–33, 1997.

[22] Jason A. Burdick and Glenn D. Prestwich. Hyaluronic acid hydrogels for biomedical applications. *Advanced Materials*, 23(12):H41–56, 2011.

[23] Jun Zhang, Bernard Senger, Dominique Vautier, Catherine Picart, Pierre Schaaf, Jean-Claude Voegel, and Philippe Lavalle. Natural polyelectrolyte films based on layer-by-layer deposition of collagen and hyaluronic acid. *Biomaterials*, 26(16):3353–3361, 2005.

[24] Jessem Landoulsi, Cécile J. Roy, Christine Dupont-Gillain, and Sophie Demoustier-Champagne. Synthesis of collagen nanotubes with highly regular dimensions through membrane-templated layer-by-layer assembly. *Biomacromolecules*, 10(5):1021–1024, 2009.

[25] J. Landoulsi, S. Demoustier-Champagne, and C. Dupont-Gillain. Self-assembled multilayers based on native or denatured collagen : mechanism and synthesis of size-controlled nanotubes. *Soft Matter*, 7(7):3337–3347, 2011.

[26] Norberto Roveri and Michele Iafisco. Evolving application of biomimetic nanostructured hydroxyapatite. *Nanotechnology, Science and Applications*, 3:107–125, 2010.

[27] R. I. Martin and P. W. Brown. Mechanical properties of hydroxyapatite formed at physiological temperature. *Nanotechnology, Science and Applications*, 6(3):138–143, 1995.

[28] Zhongkui Hong, Peibiao Zhang, Chaoliang He, Xueyu Qiu, Aixue Liu, Li Chen, Xuesi Chen, and Xiabin Jing. Nano-composite of poly(l-lactide) and surface grafted hydroxyapatite: Mechanical properties and biocompatibility. *Biomaterials*, 26(32):6296–6304, 2005.

[29] Matthew J. Meagher, Holly E. Weiss-Bilka, Margaret E. Best, Joel D. Boerckel, Diane R. Wagner, and Ryan K. Roeder. Acellular hydroxyapatite-collagen scaffolds support angiogenesis and osteogenic gene expression in an ectopic murine model: Effects of hydroxyapatite volume fraction. *Journal of Biomedical Materials Research Part A*, 104(9):2178–2188, 2016.

[30] Rafid Kasir, Varadraj N. Vernekar, and Cato T. Laurencin. Inductive biomaterials for bone regeneration. *Journal of materials research*, 32(6):1047–1060, 2017.

[31] Ruixue Sun, Kezheng Chen, Zhongmiao Liao, and Nan Meng. Controlled synthesis and thermal stability of hydroxyapatite hierarchical microstructures. *Materials Research Bulletin*, 48(3):1143–1147, 2013.

[32] Hae-Won Kim, Hae-Hyoung Lee, and J. C. Knowles. Electrospinning biomedical nanocomposite fibers of hydroxyapaite/poly(lactic acid) for bone regeneration. *Journal of Biomedical Materials Research Part A*, 79(3):643–649, 2006.

[33] Alon Elyada, Nissim Garti, and Helga Füredi-Milhofer. Polyelectrolyte multilayer-calcium phosphate composite coatings for metal implants. *Biomacromolecules*, 15(10):3511–3521, 2014.

[34] Anna Tampieri, Giancarlo Celotti, Elena Landi, Monica Sandri, Norberto Roveri, and Giuseppe Falini. Biologically inspired synthesis of bone-like composite: Self-assembled collagen fibers/hydroxyapatite nanocrystals. *Journal of Biomedical Materials Research Part A*, 67A(2):618–625, 2003.

[35] Peixin Zhu, Yoshitake Masuda, and Kunihito Koumoto. The effect of surface charge on hydroxyapatite nucleation. *Biomaterials*, 25(17):3915–3921, 2004.

[36] Mehdi Sadat-Shojai, Mohammad-Taghi Khorasani, Ehsan Dinpanah-Khoshdargi, and Ahmad Jamshidi. Synthesis methods for nanosized hydroxyapatite with diverse structures. *Acta Biomaterialia*, 9(8):7591–7621, 2013.

[37] Hye-Sun Yu, Jun-Hyeog Jang, Tae-Il Kim, Hae-Hyoung Lee, and Hae-Won Kim. Apatite-mineralized polycaprolactone nanofibrous web as a bone tissue regeneration substrate. *Journal of Biomedical Materials Research Part A*, 88A(3):747–754, 2009.

[38] Mayumi Iijima, Yutaka Moriwaki, Ryozo Yamaguchi, and Yoshinori Kuboki. Effect of solution ph on the calcium phosphates formation and ionic diffusion on and through the collagenous matrix. *Connective Tissue Research*, 36(2):73–83, 1997.

[39] Jung-Ju Kim, Ja-Yeon Lee, and Hae-Won Kim. Hydroxyapatite mineral tubes developed for the loading and release of biological proteins. *Materials Letters*, 167:170–174, 2016.

[40] Balasaheb B. Chandanshive, Priyanka Rai, Andre L. Rossi, Ovidiu Ersen, and Deepa Khushalani. Synthesis of hydroxyapatite nanotubes for biomedical applications. *Materials Science and Engineering C*, 33:2981–2986, 2013.

[41] Sandra C. Rodrigues, Christiane L. Salgado, Abhishek Sahu, Monica P. Garcia, Maria H. Fernandes, and Fernando J. Monteiro. Preparation and characterization of collagen-nanohydroxyapatite biocomposite scaffolds by cryogelation method for bone tissue engineering applications. *Journal of Biomedical Materials Research Part A*, 101(4):1080–1094, 2013.

[42] Masanori Kikuchi. Hydroxyapatite/collagen bone-like nanocomposite. *Biological and Pharmaceutical Bulletin*, 36(11):1666–1669, 2013.

[43] Masanori Kikuchi, Soichiro Itoh, Shizuko Ichinose, Kenichi Shinomiya, and Junzo Tanaka. Self-organization mechanism in a bone-like hydroxyapatite/collagen nanocomposite synthesized in vitro and its biological reaction in vivo. *Biomaterials*, 22(13):1705–1711, 2001.

[44] Fu-Zhai Cui, Yan Li, and Jun Ge. Self-assembly of mineralized collagen composites. *Materials Science and Engineering R*, 57(1-6):1–27, 2007.

[45] Irina M. Pelin, Stelian S. Maier, Gabrielle C. Chitanu, and Victor Bulacovschi. Preparation and characterization of a hydroxyapatite–collagen composite as component for injectable bone substitute. *Materials Science and Engineering C*, 29(7):2188–2194, 2009.

[46] Benjamin Thierry, Françoise M. Winnik, Yahye Merhi, Jim Silver, and Maryam Tabrizian. Bioactive coatings of endovascular stents based on polyelectrolyte multilayers. *Biomacromolecules*, 4(6):1564–1571, 2003.

[47] Royal Society of Chemistry. Hyaluronic acid. `http://www.chemspider.com/Chemical-Structure.2341173.html`, 2015. [Online; accessed 03-June-2017].

[48] Harold P. Erickson. Size and shape of protein molecules at the nanometer level determined by sedimentation, gel filtration, and electron microscopy. *Biological Procedures Online*, 11(1):32–51, 2009.

Rue Archimède, 1 bte L6.11.01, 1348 Louvain-la-Neuve **www.uclouvain.be/epl**